FACULTAD DE CIENCIAS DEL MAR

UNIVERSIDAD DE LAS PALMAS DE GRAN CANARIA

Increasing or decreasing trends in primary production in the Canary Current upwelling system? - A regional perspective

Markel Gómez Letona

Curso 2015/2016

Javier Arístegui Ruiz

Antonio Juan González Ramos

Trabajo Fin de Título para la obtención del título de graduado en Ciencias del Mar.

Título del TFT: *Increasing or decreasing trends in primary production in the Canary Current upwelling system? - A regional perspective*.

Trabajo de fin de título presentado por Markel Gómez Letona para la obtención del título de graduado en Ciencias del Mar por la Universidad de Las Palmas de Gran Canaria.

El presente trabajo fue dirigido por:

Dr. Javier Arístegui Ruiz, Instituto de Oceanografía y Cambio Global (IOCAG), Universidad de Las Palmas de Gran Canaria.

Dr. Antonio Juan González Ramos, división de robótica y oceanografía computacional del Instituto Universitario de Sistemas Inteligentes y Aplicaciones Numéricas en la Ingeniería (SIANI), Universidad de Las Palmas de Gran Canaria.

Firma del estudiante | Firma de los tutores

En Las Palmas de Gran Canaria, a 8 de julio de 2016

Table of contents

Abstract

After Bakun (1990) proposed his hypothesis of upwelling intensification caused by increasing global warming, contradictory results have been published on whether primary productivity is increasing or decreasing in Eastern Boundary Upwelling Ecosystems (EBUE). The present work is focused in comparing two net primary production (NPP) models (the Eppley-VGPM and the CbPM), derived from remote sensing data, in the Canary Current EBUE during the 1998-2007 period. We looked for seasonal to interannual trends of NPP under a regional perspective, with the aim of searching for temporal patterns that could support or reject the intensification hypothesis. According to previous studies based on the seasonality of the upwelling regime, the CanC EBUE was divided into three subregions: a seasonal upwelling zone (SUZ; 13-20ºN), a permanent upwelling zone (PUZ; 20-26ºN) and a weak permanent upwelling zone (WPUZ; 26-33ºN). Our analyses did not show significant increasing trends in NPP with any of the two productivity models used, challenging Bakun's hypothesis. Nevertheless, differences in the output of the two models where significant, both at regional and subregional scales, questioning the accuracy of the models. NPP was compared with proxies of upwelling drivers (Sea-surface temperature, Ekman pumping, nutrients) and community structure (phytoplankton functional groups). Overall, correlations with nutrients and phytoplankton yielded no consistent results, possibly due to the lack of spatial accuracy of these models. Sea-surface temperature, however, showed correlations with some climate indices although varied depending on the time period selected. This disparity of results is also frequently found in the literature, emphasizing the importance of the time period used and the datasets selected, not only for the calculation of correlations, but also for the estimation of trends.

Key words

Canary Current EBUE, Upwelling, NPP and Chl-*a*, Phytoplankton functional groups, Decadal trends, Climate indices.

1. Introduction

Over the recent decades increasing trends in global warming have been evident in most oceanic regions, both at surface and deep layers (Levitus et al., 2000; Gille, 2002; Levitus et al., 2005; Ihara et al., 2008; Hansen et al., 2010; Gouretski et al., 2012; Nieves et al., 2015). Impacts of rising temperatures on marine ecosystems may have direct effects on the ranges of distribution and vulnerability of organisms, but also on the productivity of ecosystems, their management and their services (IPCC WGII AR5). Ocean surface warming leads to enhanced stratification of the water column, reducing vertical mixing and hence limiting the supply of colder, nutrient-enriched waters to the euphotic zone, where primary production takes place. Behrenfeld et al. (2006) were the first to provide evidence of a reduction on global average net primary production (NPP), derived from remote sensing ocean-colour data, of 190 TgC·year^{-1} for the 1999-2006 period, associated with a global warming trend during the same period. Boyce et al. (2010) combined in situ chlorophyll *a* (Chl-*a*) measurements with sea water transparency to found also a global significant decline of Chl-*a* (about -0.020 mg·m^{-3}·ºC^{-1}) over the 20th century, related to increasing sea surface temperatures. Nevertheless, other authors have found both increasing and decreasing trends on phytoplankton biomass and primary productivity, related to multi-decadal climatic oscillations over the last century, showing variable regional patterns (Martinez et al., 2009; Chavez et al. 2011). Overall, present observations suggest that NPP will increase with global warming at high latitudes, but this enhancement will be offset by a decrease at open-ocean temperate and tropical latitudes. Moreover, the poor and uncertain information on the productivity trends at coastal and near-shore regions, which largely contribute to the global productivity, reduce confidence in future global projections (IPCC WGII AR5). Indeed, although the global ocean is projected to warm under climate change, the surface waters of eastern boundary upwelling ecosystems (EBUE) – contributing nearly 25% to global fish production- may lead to cooling rather than warming, causing enhanced productivity. Bakun (1990) proposed that EBUE would tend to cool, as the result of the intensification of wind-driven upwelling. According to his hypothesis, the stronger continental land mass warming compared to the ocean would cause an increase in the cross-shore atmospheric pressure gradient, intensifying coastal upwelling, hence enhancing primary productivity. Analysis of sea-surface temperatures, wind trends and chlorophyll provide however contradictory evidences to support Bakun's hypothesis in all EBUEs (Snyder et al., 2003; McGregor et al., 2007; Demarcq, 2009; Narayan et al., 2010; Barton et al., 2013; Cropper et al. 2014; Sydeman et al., 2014; Oerder et al., 2015; Varela et al., 2015; Wang et al., 2015). Moreover, it is unclear to what extent wind stress can offset the increased stratification in upwelling regions due to surface warming, and how other ecosystem drivers (like the progressive acidification and deoxygenation) could affect organisms' responses and ecosystem productivity in EBUEs.

The present work aims to shed some light on this controversy by analysing spatiotemporal trends on physical and biological variables in the CanC upwelling region, one of the four major EBUEs in the planet, along with the California, Humboldt and Benguela systems (Carr and Kearns, 2003; Chavez and Messié, 2009). Use of both satellite and modelling data has been made to explore seasonal to interannual trends in sea-surface temperature, Ekman pumping, nutrients, chlorophyll, primary production, and phytoplankton functional groups, for the 1998-2007 period. Past observations indicate that the CanC has been warming at both local and regional scales since the early 1980s, with a decrease in chlorophyll over the last two decades (Arístegui et al., 2009; Belkin, 2009; Demarcq, 2009). In this study we have further extended the analyses to sub-regional scales, exploring the impact of global warming on phytoplankton functional groups, looking at correlations with climatic indices from the Pacific and Atlantic Oceans.

The CanC region displays a great geographical variability, resulting in highly diverse upwelling environments (Arístegui et al., 2009). Nevertheless, for the purpose of this study three main sub-regions have been identified according to their upwelling intensity throughout the year, following the description made by Cropper et al. (2014), that distinguishes: a seasonal upwelling zone (SUZ) along the Senegalese-Mauritanian coast, which expands from 13 to 20ºN, a permanent upwelling zone (PUZ), from 20 to 26ºN and a weak permanent upwelling zone (WPUZ), from 26 to 33ºN (Fig. 1). Notice, however, that these latitudinal bands represent approximate boundaries, as in practice they might vary from year to year due to the meridional shift of the Trade wind system.

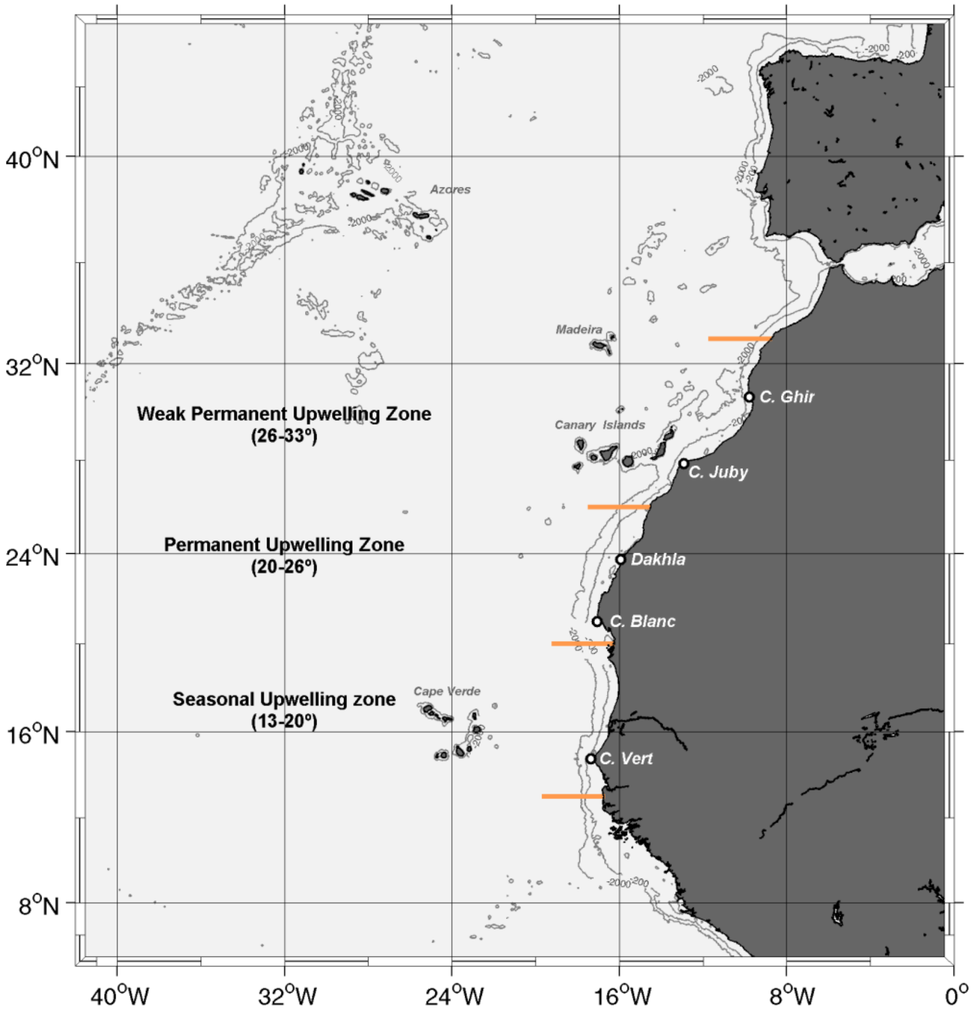

Fig. 1. CanC upwelling region and its main geographical features. The three upwelling subregions, namely, the weak permanent (WPUZ), permanent (PUZ) and seasonal upwelling zones (SUZ), are separated by lines. 200m and 2000 m isobaths are represented by grey contour lines. Bathymetry data corresponds to a 2' global dataset derived by Smith and Sandwell (1997).

2. Data and methods

Most of the variables used in this study were derived from remote sensing data, while some of them were inferred from a biogeochemical model approach. The variables are: Sea-surface temperature (SST), Ekman pumping, inorganic nutrients, chlorophyll *a* (Chl-*a*), net primary production (NPP), and phytoplankton functional groups. The time period covered by all datasets extends from 01/1998 to 12/2007 except for the Ekman pumping dataset, which includes only the 01/2000 to 12/2007 period.

2.1. Seas-surface temperature (SST)

SST from daily Reynolds analysis at a spatial resolution of ¼º and weekly temporal resolution was provided by the Copernicus Marine Environment Monitoring Service (CMEMS) at http://marine.copernicus.eu/ (ref. GLOBAL_REP_PHYS_001_013). The dataset combines AVHRR and in situ data.

2.2. Ekman pumping

Ekman pumping consists in an upward/downward flow in the water column due to wind curl. Data employed at the present work was derived by Coca et al. (2006) from QuikSCAT L2B datasets at a spatial resolution of about 1/9º and at a daily temporal resolution. The daily data correspond to 5-day global means (each day and the previous 4) as they were processed in order to cover gaps left by observation swaths, especially near the equator. As QuikSCAT data are only available from 09/1999, Ekman pumping data extend over 8 years (from 01/01/2000 to 31/12/2007). QuikSCAT datasets were obtained from the Physical Oceanography Distributed Active Archive Center (PODAAC) portal of the NASA's Jet Propulsion Laboratory: http://podaac.jpl.nasa.gov/.

Ekman pumping was derived from wind speeds (see supplementary material for a detailed description of the procedure) and is defined by the following expression:

$$W_E = \frac{1}{\rho_w f}\left(\frac{\partial \tau_y}{\partial x} - \frac{\partial \tau_x}{\partial y}\right) \qquad (1)$$

where ρ_w is the water density, f the Coriolis parameter and τ_x and τ_y are the zonal and meridional wind stress components, respectively.

The above expression implies that when wind curl is positive (negative) Ekman pumping (W_E) is also positive (negative), i.e., there is an upward (downward) transport of water.

2.3. Nutrients

Datasets corresponding to four nutrients −iron (Fe), biogenic silica (Si), nitrates and phosphates− were provided by the Copernicus Marine Environment Monitoring Service (CMEMS; ref. GLOBAL_REANALYSIS_BIO_001_018) at a variable spatial resolution, being of 1/4º at the equator. Nutrient concentrations are non-assimilative hindcast simulations derived from the Pelagic Interactions Scheme for Carbon and Ecosystem Studies (PISCES) biogeochemical model (Aumont and Bopp, 2006; Aumont et al., 2015). The model has 24 prognostic variables (including two phytoplankton and zooplankton components) and simulates the biogeochemical cycles of several key nutrients found in the ocean. A detailed description of the model can be found at Aumont and Bopp (2006).

2.4. Chlorophyll-a (Chl-a)

SeaWiFS (Sea-Viewing Wide Field-of-View Sensor) Chl-*a* was chosen because is one of the longest ocean colour time series available and coincides with the time periods available for the rest of the datasets. It was provided by the Oregon State University (OSU) at their portal: http://www.science.oregonstate.edu/ocean.productivity/. The data were from the SeaWiFS.r2010 reprocessing results, with a temporal resolution of 8 days and a spatial resolution of 1/12º.

Chl-*a* was used as a proxy for phytoplankton biomass, although it has to be noted that the "Carbon:Chl-*a* ratio" may vary among different species of phytoplankton as well as their metabolic states.

2.5. Net Primary Production (NPP)

The main goal of this study is to look at seasonal to decadal trends in productivity in the CanC region. For this purpose two of the most well-known NPP models were selected to compare them: the Eppley-VGPM (Vertically Generalized Production Model) and the CbPM (Carbon-based Production Model), both provided by the OSU. The Eppley-VGPM is a SeaWiFS-Chl-based model, with a temporal resolution of 8 days and a spatial resolution of 1/12º. It represents a modified version of the VGPM developed by Behrenfeld and Falkowski (1997a), replacing the original polynomial description of the variation of light-saturated photosynthetic efficiencies, based on daily integrated production measurements (P^{B}_{opt}), with the exponential function described by Morel (1991), based on the curvature of the temperature-dependent growth function of Eppley (1972). NPP is derived from Chl-*a*, SST, photosynthetically active radiation (PAR) and day length.

The CbPM was developed by Behrenfeld et al. (2005) and modified by Westberry et al. (2008), and is based on particulate backscattering coefficients (b_{bp}) and phytoplankton absorption coefficients. Phytoplankton carbon biomass is estimated from b_{bp}, while phytoplankton absorption coefficients are used to evaluate the Chl:carbon ratios which in turn are employed to derive growth rates, and all together to infer NPP.

A more detailed description of the models can be found at the OSU portal mentioned above.

2.6. Phytoplankton functional groups

Phytoplankton functional groups' concentrations derived from the NASA Ocean Biogeochemical Model (NOBM) were supplied, at a spatial resolution of 2/3º in latitude and 1.25º in longitude and at a temporal resolution of 1 day, by the old Giovanni portal (the new one can be found at http://giovanni.gsfc.nasa.gov/giovanni/). This dataset corresponds to the R2012.3 reprocessing version.

The NOBM is a 3-dimensional global oceanic model that includes components accounting for circulation dynamics, biogeochemical processes and radiative transfer (Gregg and Casey, 2007). The biogeochemical model contains four phytoplankton groups, four nutrients, one herbivore group and three detrital pools (Gregg, 2008). The four phytoplankton groups (diatoms, coccolithophores, cyanobacteria and chlorophytes) differ in maximum growth rates, sinking rates, nutrient requirements and optical properties. Chlorophytes are intended to represent prasinophytes, pelagophytes and other nanoflagellates, while cyanobacteria stands for all prokaryotic picophytoplankton (Gregg et al., 2003). A detailed description of the model can be found in Gregg et al. (2003) and Gregg (2008).

2.7. Linear fits

In order to estimate the change rate of the different variables throughout the time period analysed, linear fits were computed. The first approach was to use the least squares (LS) method, but it had to be rejected as residuals of linear regressions of several variables did not fulfil the required conditions of normality and homoscedasticity. Therefore, the Theil-Sen slope estimator was chosen as an alternative, since it is a robust method against outliers that generate departures from normality and homoscedasticity of the residuals. The method, developed by Theil (1950) and later extended by Sen (1968), yields a simple linear regression of a set of data points, estimating the median slope among all lines connecting pairs of points. Although it is a robust method, correction for temporal autocorrelation is required to correctly estimate the significance of the calculated slopes. This was achieved making use of the modified Mann-Kendall trend test developed by Hamed and Rao (1998), which corrects Mann-Kendall test Z statistics and, consequently, p-values for autocorrelated data. The significance boundary was set at the usual 0.05

level. Besides, the percentage of change was estimated making use of the first and last data points of each linear fit.

2.8. Correlations

As datasets in the present work exhibit departures from normality and extreme values, Spearman's rank correlation coefficient (also known as Spearman's ρ) was used, a nonparametric method that is robust to outliers. Spearman's ρ ranges values between -1 and +1 depending on how close are two variables of being monotonic functions of each other. Note that this is different comparing with the more common Pearson product-moment correlation coefficient, in which perfect values of either -1 or +1 are only achieved when the two variables are related by a linear function. A positive value of Spearman's ρ indicates that a direct relationship between the two variables exists. On the other hand, a negative value implies that an inverse association is present and a value equal to zero means that no relation exists. The significance boundary chosen was the usual 0.05 level. However, correlations with significance less than 0.1 were also considered (as nearly significant) due to the shortness of the time quarterly series.

2.9. Seasonal climatological anomalies

Seasonal climatological anomalies were estimated within each upwelling subregion to better study fluctuations of the different variables and thus support trend analysis. The areas selected are shown in Fig. 2. The box approach was chosen taking into account the scarce spatial resolution of some datasets, and in order to include the oceanward extensions of the coastal upwelling.

The procedure followed for their computation involved three steps: 1) Averaging datasets in order to obtain seasonal time series, dividing each year into four quarters: (i) Winter, corresponding to January, February and March (JFM); (ii) Spring, corresponding to April, May and June (AMJ); (iii) Summer, corresponding to July, August and September (JAS); and (iv) Autumn, corresponding to October, November and December (OND); 2) Calculating mean values for each season over the whole time series; and 3) Subtracting the corresponding seasonal climatology from each measured seasonal value. In order to estimate the anomalies for all the three upwelling subregions, datasets were also spatially averaged prior to the computation of climatologies. Besides, correlations between NPP model anomalies and the other variables were estimated in order to search for dependencies.

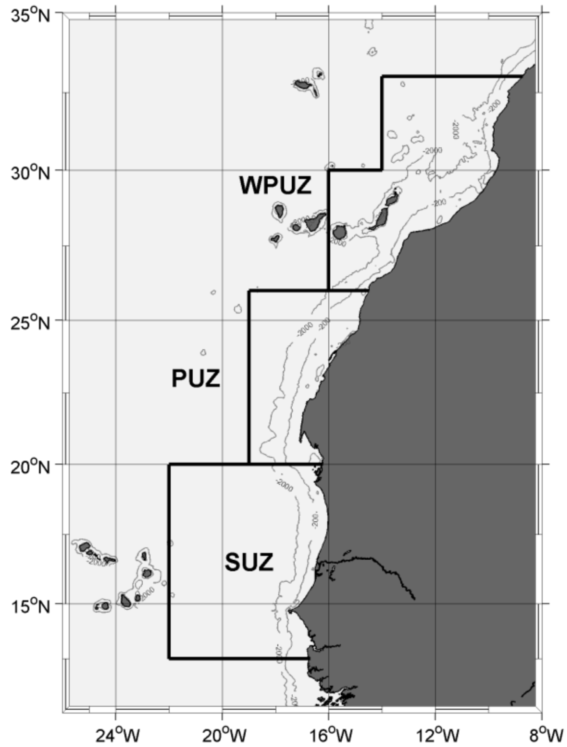

Fig. 2. Geographical domains selected to spatially average datasets. Acronyms stand for weak permanent upwelling zone (WPUZ), permanent upwelling zone (PUZ) and seasonal upwelling zone (SUZ).

2.10. Climate-related variability

Five climate indices were selected to look at correlations with the studied variables:

- The Multivariate ENSO Index (MEI) and the Southern Oscillation Index (SOI). Although MEI and SOI both describe the El Niño-Southern Oscillation (ENSO) they do it in distinct ways: while SOI is based on the observed sea-level pressure (SLP) differences between Tahiti and Darwin (Australia), MEI takes six observed variables into account: SLP, zonal and meridional components of the surface wind, SST, surface air temperature and total cloudiness fraction of the sky. Despite the fact that MEI and SOI characterise the same phenomena both are analysed so as to be able to make stronger assumptions supported by two different indexes. MEI and SOI were obtained from the National Oceanic and Atmospheric Administration (NOAA) databases (http://www.esrl.noaa.gov/psd/enso/mei/ and https://www.ncdc.noaa.gov/teleconnections/enso/indicators/soi/, respectively).
- The station-based North Atlantic Oscillation (NAO-SB) and the principal component-based North Atlantic Oscillation (NAO-PC). The NAO-SB is based on the difference of normalized SLP between Lisbon (Portugal) and Stykkisholmur/Reykjavik (Iceland) whereas the NAO-PC is the leading Empirical Orthogonal Function (EOF) of the SLP anomalies over the ocean area covered between 20°-80°N and 90°W-40°E. Like with MEI/SOI, two different indices for

the same mode of variability are chosen in order to support a more consistent analysis. Both NAO indexes were provided by the National Center for Atmospheric Research (NCAR) at https://climatedataguide.ucar.edu/climate-data.

- The Eastern Atlantic Pattern (EA) represents a southward-displaced NAO-like index. It also consists of a north-south dipole of anomalies, though these are shifted southeastward relative to those of NAO. Nevertheless, the south centre of the dipole has a strong subtropical link related to the variations of the subtropical ridge. This fact differentiates the EA from the NAO and makes it possibly more suitable to characterise the variability of the CanC upwelling as it is located in subtropical latitudes. EA was also obtained from the NOAA database at http://www.cpc.ncep.noaa.gov/data/teledoc/ea.shtml.

Following the same approach as Arístegui et al. (2006), correlations between ENSO indices and the different variables were searched comparing the 1st and 2nd quarter of a year of each variable with the 4th quarter of the previous year of the SOI/MEI, since this quarter tends to exhibit the greatest correlations. Correlations were also calculated independently for each of the quarters with no lag applied for all the five indices to assess if short-term responses exist. Additionally, correlations were estimated for the 1993-2014 time period in the case of SST, as discussed in section 4.3. Finally, correlations were also estimated for the entire time series with no distinction of quarters, applying time lags each three months, from zero to one year delay, being the climate indices always the leading parameter.

3. Results

3.1 Linear trends

3.1.1 Trends in SST

Trends computed with SST data overall showed a significant ($p<0.001$) warming tendency south of 30ºN (even reaching as much as 1 ºC·decade^{-1}) and no significant increase of SST north of 30ºN for the 1998-2007 time period (Fig. 3). Nevertheless, attending to regional variations differences could be identified between some zones. Oceanic waters south of 30ºN presented a mean warming trend of 0.93 ºC·decade^{-1} whereas waters of the shelf portion of the upwelling zone showed a mean increase of 0.81 ºC·decade^{-1}, with patches of either significant ($p<0.001$) warming or non-significant SST trend. The most important patches showing no significant SST trends expanded alongshore from Cape Vert to Cape Blanc and, to a lesser extent, around and north of Cape Juby. North of 30ºN gentler, non-significant trends were registered: the open ocean and shelf warmed at a rate of 0.41 ºC·decade^{-1} and 0.29 ºC·decade^{-1}, respectively.

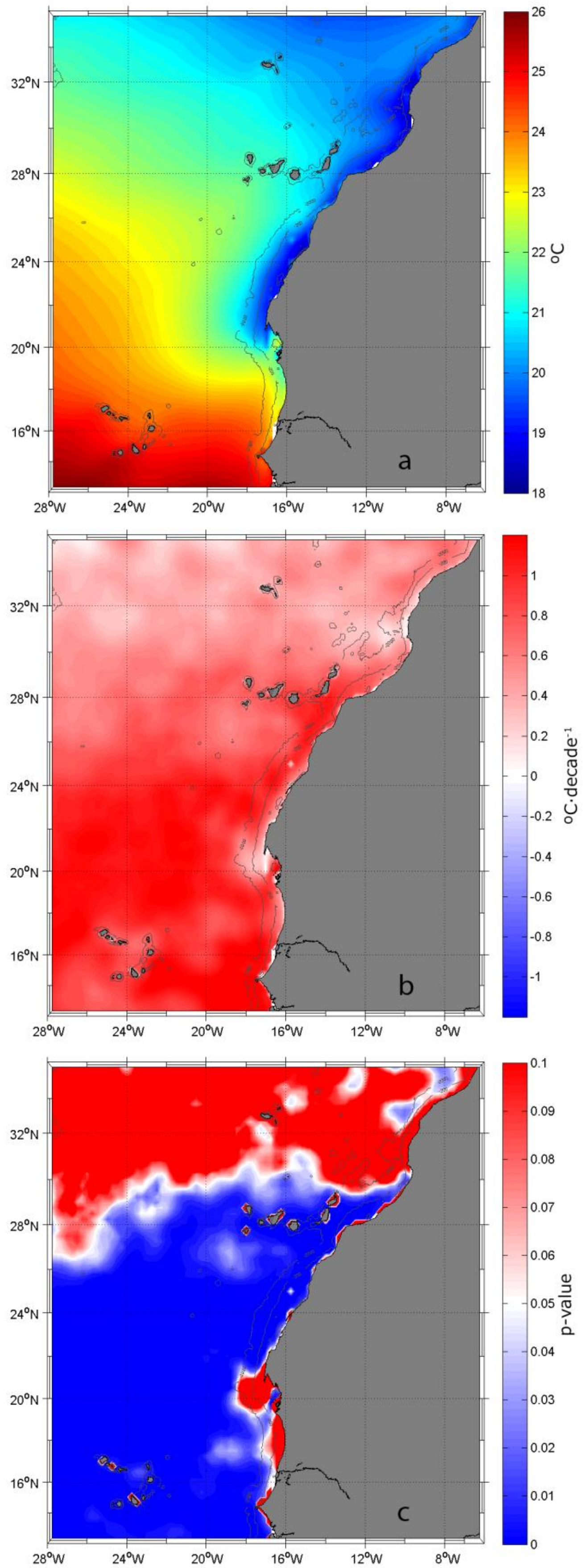

Fig. 3. Mean SST (a), SST trend (b) and trend significance (c) for the 1998-2007 period. In (c) blue corresponds to significant trends and red to non-significant trends. 200m and 2000m isobaths are represented by grey contour lines.

In regard to SST trends in each of the upwelling subregions (Table 1), SUZ and PUZ presented similar warming trends (0.78 and 0.70 ºC·decade^{-1}, respectively). The WPUZ exhibited a lower trend with an average increase of 0.61 ºC·decade^{-1}.

Area		**SST [ºC·decade^{-1}] (%)**	**SeaWiFS Chl-*a* [mgChl·m^{-3}] (%)**	**Eppley-VGPM [mgC·m^{-2}·decade^{-1}] (%)**	**CbPM [mgC·m^{-2}·decade^{-1}] (%)**
Weak permanent upwelling zone	**Shelf**	**0.618 (3.26)****	-0.152 (-10.38)	6.2 (0.50)	**-470.2 (-36.91)****
	Slope	**0.649 (3.30)****	-0.041 (-12.30)	-9.8 (-1.93)	**-113.3 (-18.85)****
	Open-ocean	0.527 (2.52)	-0.011 (-10.21)	-14.8 (-5.03)	4.7 (1.27)
Permanent upwelling zone[a]	**Shelf**	**0.699 (3.65)****	-0.085 (-2.66)	43.1 (1.99)	*-610.8 (-43.76)**
	Slope	**0.845 (4.28)****	0.003 (0.19)	18.6 (1.32)	163.4 (16.43)
	Open-ocean	**0.998 (4.51)****	-0.074 (-22.73)	-78.5 (-13.66)	*50.9 (9.57)**
Seasonal upwelling zone[a]	**Shelf**	*0.782 (3.49)**	-0.527 (-10.18)	20.1 (0.60)	76.0 (7.10)
	Slope	**0.931 (3.98)****	-0.546 (-25.99)	-216.7 (-12.18)	125.7 (12.05)
	Open-ocean	**1.063 (4.50)****	-0.264 (-40.27)	-175.7 (-19.10)	-87.9 (-10.33)

Table 1. Average trends for SST, Chl-*a* and NPP (Eppley-VGPM and CbPM) and changes in percentage for the 1998-2007 period in each of the upwelling subregions over the shelf (0-200m), continental slope (200-2000m) and open-ocean region (>2000m, as far as 28ºW). Significance reads as follows: ($p<0.01$): **bold****, ($p<0.05$): *italics**. [a] Banc d'Arguin zone was excluded from the mean estimates due to its special characteristics (shallow, warm waters with high turbidity).

3.1.2 Trends in NPP and Chl-a

NPP trends computed from the Eppley-VGPM and CbPM showed very different patterns. The highest changes in the Eppley-VGPM trends were mainly located in the SUZ with a mean increase of about 20 mgC·m^{-2}·decade^{-1} (Table 1), although two different regions could be clearly identified: one with an increasing trend around Cape Blanc (with peaks over 800 mgC·m^{-2}·decade^{-1}) and the other with a decreasing trend north of Cape Vert, being the boundary between them at 17-18ºN (Fig. 4). Nevertheless, note that only in some patches the trends are significant ($p<0.001$). Besides, even though not being significant, it is worthwhile remarking the broad open ocean area showing a decrease in NPP off the SUZ. Regarding the two other upwelling subregions, both presented zones of slight increase/reduction of NPP. Average trend values for PUZ and WPUZ were around 45 and 5 mgC·m^{-2}·decade^{-1}, respectively; although they are not significant.

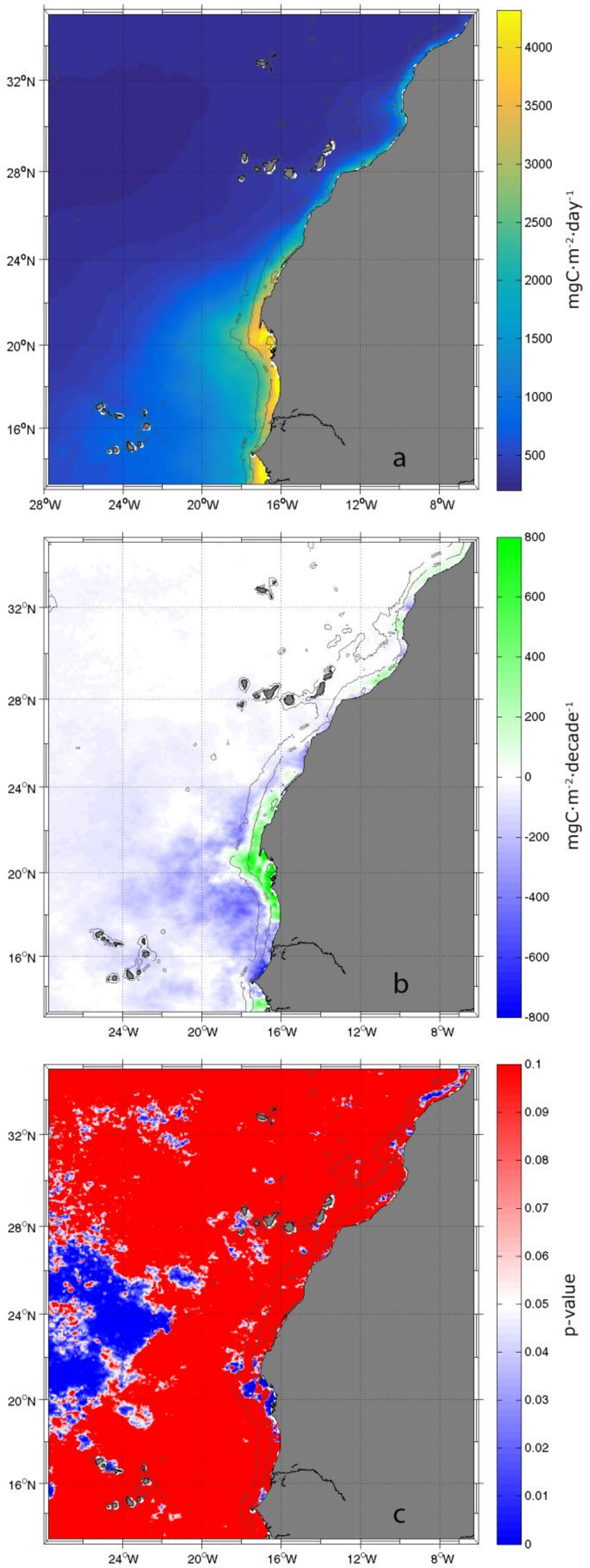

Fig. 4. Mean Eppley-VGPM (a), Eppley-VGPM trend (b) and trend significance (c) for the 1998-2007 period. In (c) blue corresponds to significant trends and red to non-significant trends. 200m and 2000m isobaths are represented by contour lines.

In general, the CbPM exhibited more marked trends than the Eppley-VGPM (Fig. 5). Furthermore, there were major differences in the spatial distribution of trends between the two NPP models. The CbPM showed a strong average decreasing trend of -470 $mgC·m^{-2}·decade^{-1}$ (although exceeding -800 $mgC·m^{-2}·decade^{-1}$ in relatively broad areas) with a high statistical significance ($p<0.001$) in the WPUZ (Fig. 5). The PUZ presented a similar significant decreasing trend for the most part of the region, with average values of -610 $mgC·m^{-2}·decade^{-1}$. On the other hand, the SUZ showed a positive average trend (75 $mgC·m^{-2}·decade^{-1}$). In fact, there was a highly significant ($p<0.001$) positive trend off Cape Blanc, with broad areas reaching 500 $mgC·m^{-2}·decade^{-1}$. This yields positive mean trends over the continental slope around Cape Blanc, both in the SUZ (125 $mgC·m^{-2}·decade^{-1}$) and PUZ (165 $mgC·m^{-2}·decade^{-1}$) regions.

These results (Figs. 4 and 5) revealed that absolute values and trends in NPP greatly vary depending on the chosen model. A detailed comparison of the average trends in the shelf portion of each of the upwelling zones (Table 1) is shown in Fig. 6. While the CbPM presented remarkable reductions in the WPUZ and PUZ regions, the Eppley-VGPM showed no significant change, more in accordance with the Chl-*a* values. Both models only agreed in the SUZ, where NPP did not show any clear trend. Nonetheless, a common feature in both the Eppley-VGPM and CbPM was the marked seasonality of NPP in all three upwelling zones, reflecting the annual cycle in solar irradiance.

Overall Chl-*a* trends exhibited very similar patterns to those of Eppley-VGPM (see Fig. 4 and SF 1), which was expectable considering that the latter is derived from the former. The decreasing trend values differed between zones, being -0.15, -0.09 and -0.53 $mg·m^{-3}$ for SUZ, PUZ and WPUZ, respectively (Table 1 and Fig. 6).

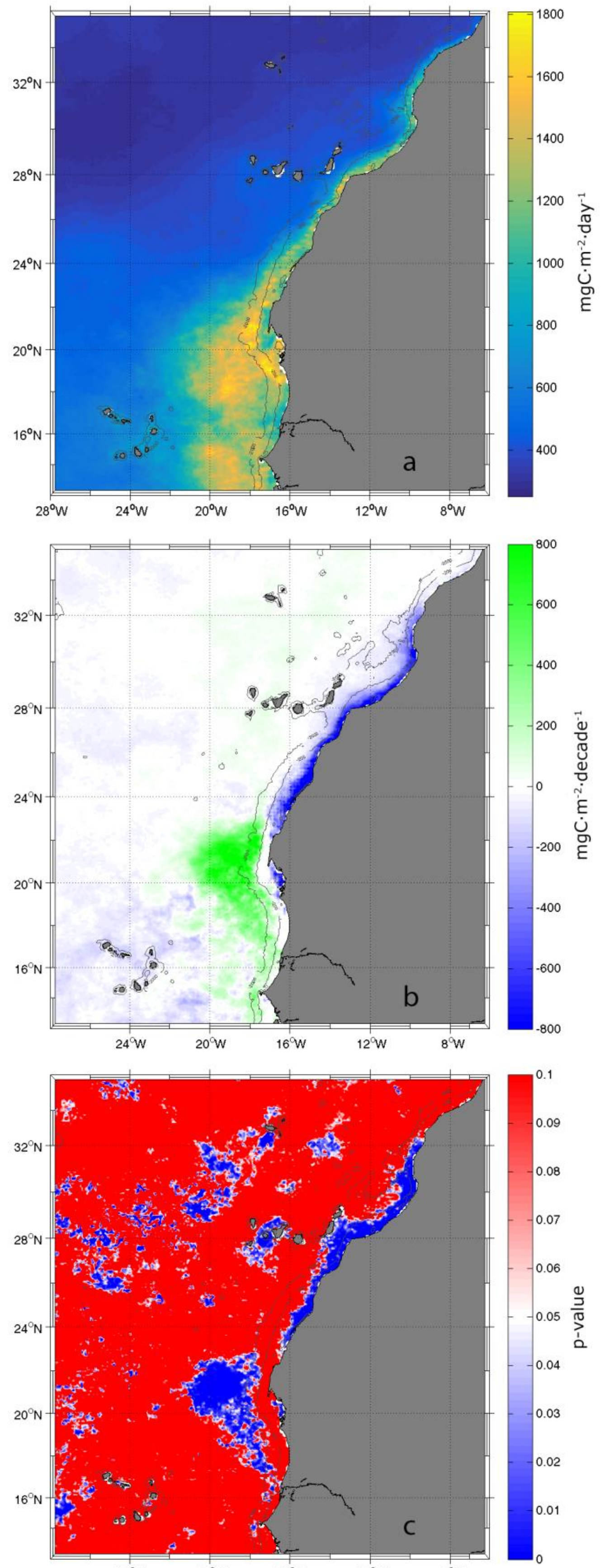

Fig. 5. Mean CbPM (a), CbPM trend (b) and trend significance (c) for the 1998-2007 period. In (c) blue corresponds to significant trends and red to non-significant trends. 200m and 2000m isobaths are represented by grey contour lines.

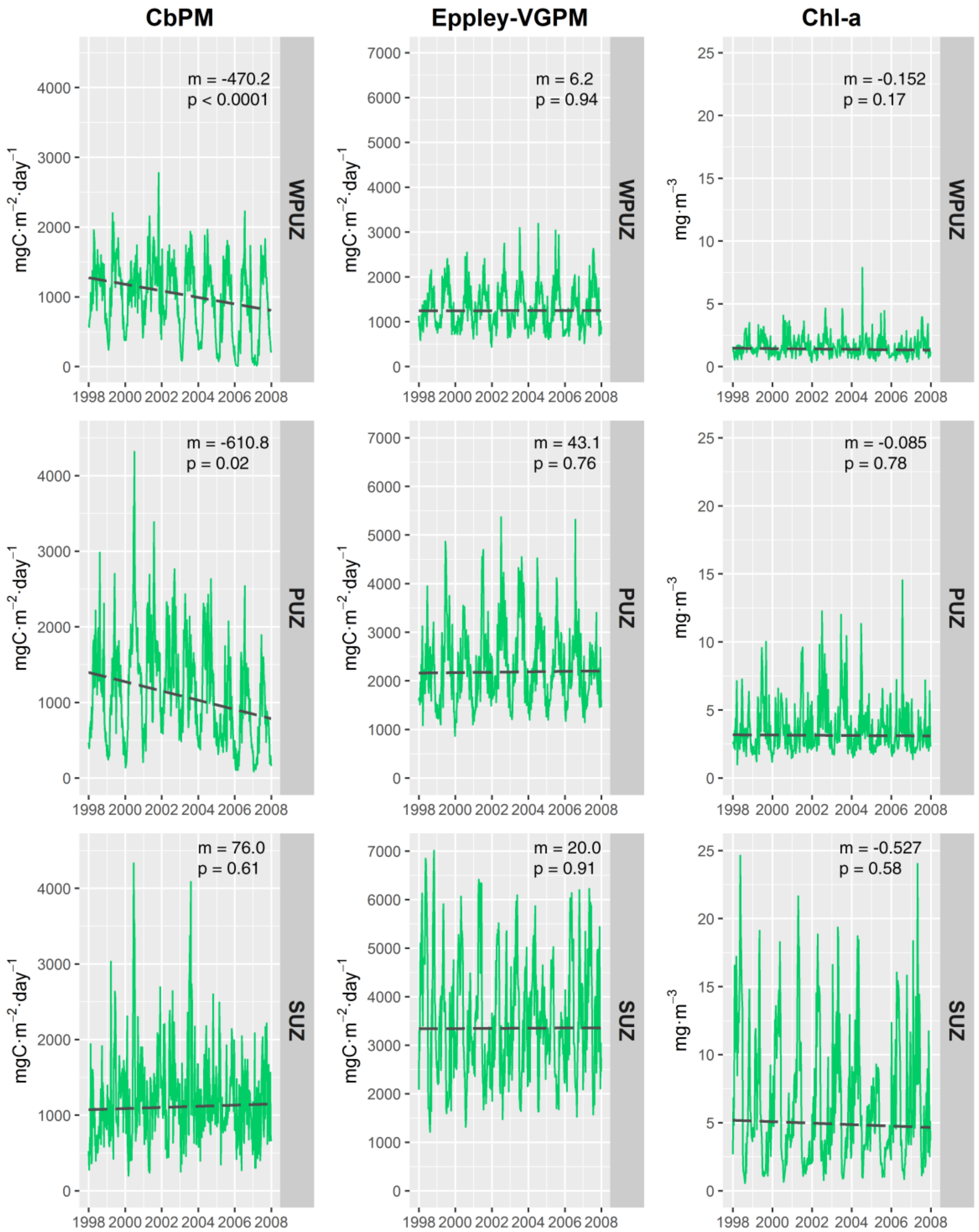

Fig. 6. Average time series in the shelf portion of each upwelling zone (green) and their corresponding trend (dashed) for CbPM, Eppley-VGPM and Chl-*a*. The slope of the fits (m) has $mgC \cdot m^{-2} \cdot decade^{-1}$ units for NPP and $mg \cdot m^{-3} \cdot decade^{-1}$ for Chl-*a*.

3.1.3 Trends in phytoplankton groups

Phytoplankton trends exhibited a shift in spatial distribution of groups. Diatoms (Fig. 7a) suffered a highly significant ($p<0.0001$) decrease of more than 0.30 $mg \cdot m^{-3} \cdot decade^{-1}$ near Dakhla, being replaced by chlorophytes (Fig. 7b) at a highly significant ($p<0.0001$) rates of about 0.30 $mg \cdot m^{-3} \cdot decade^{-1}$. The latter in turn diminished around Cape Blanc at an equally significant but varying rate of 0.10-0.30 mg·m^{-3}·decade^{-1}. Cyanobacteria presented an opposite pattern of distribution to chlorophytes, experiencing a highly ($p<0.0001$) significant increase of 0.10-0.20 mg·m^{-3}·decade^{-1} (Fig. 7c). Coccolithophores showed slight, non-significant, increases and decreases in their concentration at various locations (Fig. 7d).

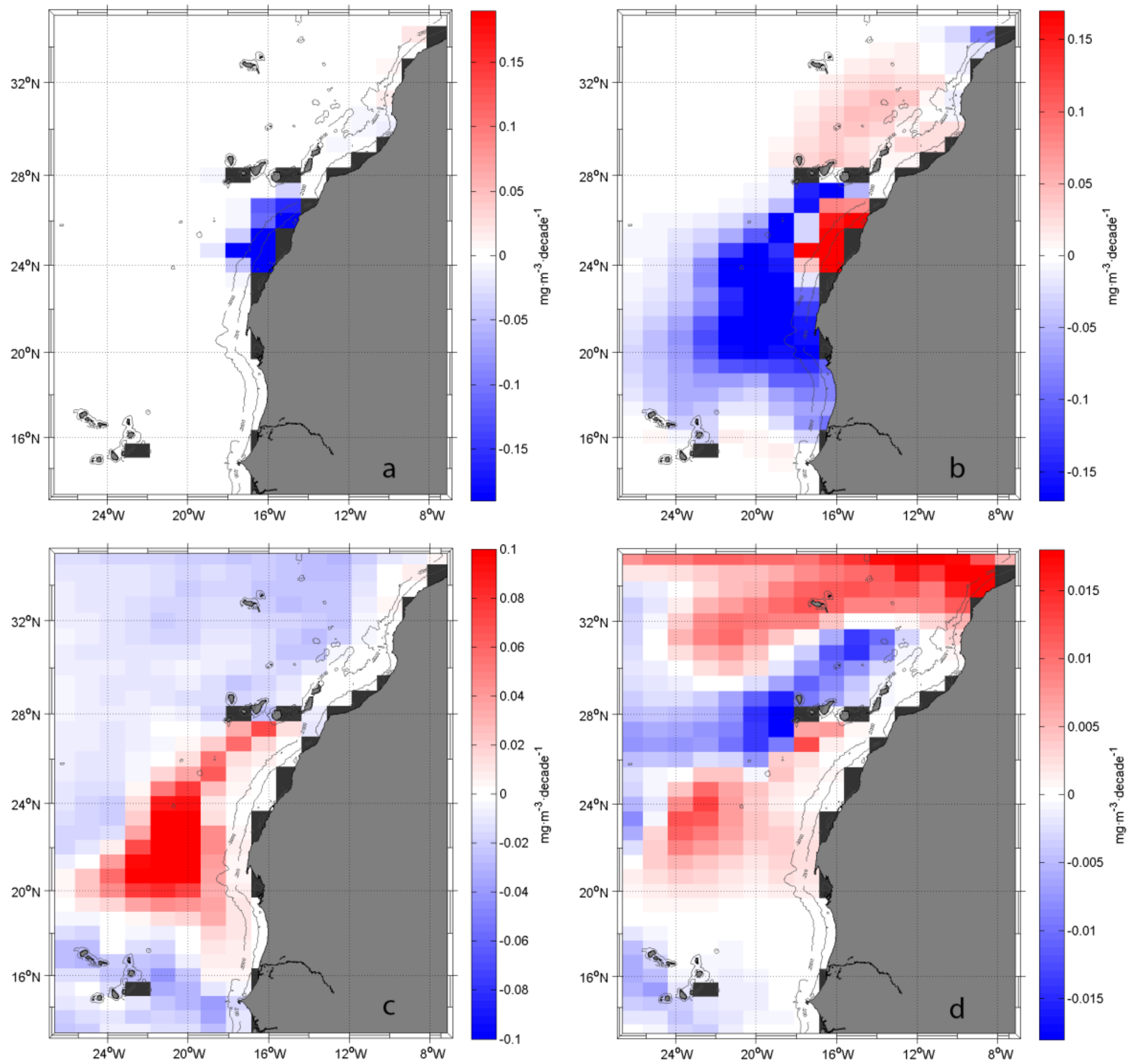

Fig. 7. Trends in phytoplankton functional groups (expressed in mgChl-*a*·m^{-3}): diatoms (a), chlorophytes (b), cyanobacteria (c) and coccolithophores (d). 200m and 2000m isobaths are represented by grey contour lines. See SF 2 for significance maps.

3.2 *Seasonal climatological anomalies*

The most apparent aspect about seasonal climatological anomalies is that, in general, there was a considerable spatial variability between the different upwelling zones studied. SST was, however, the variable which exhibits lower subregional variability (Fig. 8). In all the three zones SST anomalies (reaching or exceeding +/-0.5ºC) follow a similar pattern, with a period of negative anomalies between 1998 and 2003 (with the exception of 2002) and positive anomalies between 2003 and 2007. Ekman pumping (SF 3) presented more irregular anomalies with higher intensity in the PUZ, although not correlated with SST.

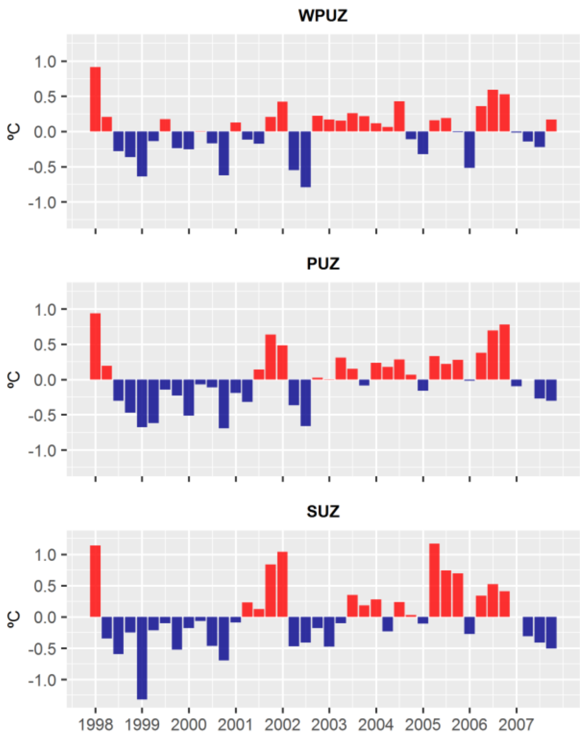

Fig. 8. Seasonal SST climatological anomalies in each upwelling zone for the 1998-2007 period.

Nutrient anomalies did not present the same variability as the beforehand mentioned. Silicates, nitrates and phosphates exhibited resembling patterns, with similar anomalies in the SUZ and PUZ and far smaller ones in the WPUZ (SF 4). On the other hand, iron displayed much the same anomalies in all the three subregions.

Seasonal anomalies of the main functional groups (Fig. 9) followed similar interannual variability than temperature, particularly in the PUZ. In this region, diatoms and chlorophytes showed opposite patterns, with positive (negative) anomalies, respectively, indicating that cold temperatures (1998-2003) favour the growth of diatoms, while warmer temperatures (2003-2008) shift the community to small flagellates (chlorophytes). Likewise, cyanobacteria showed positive anomalies during the warmer period both in the PUZ and SUZ.

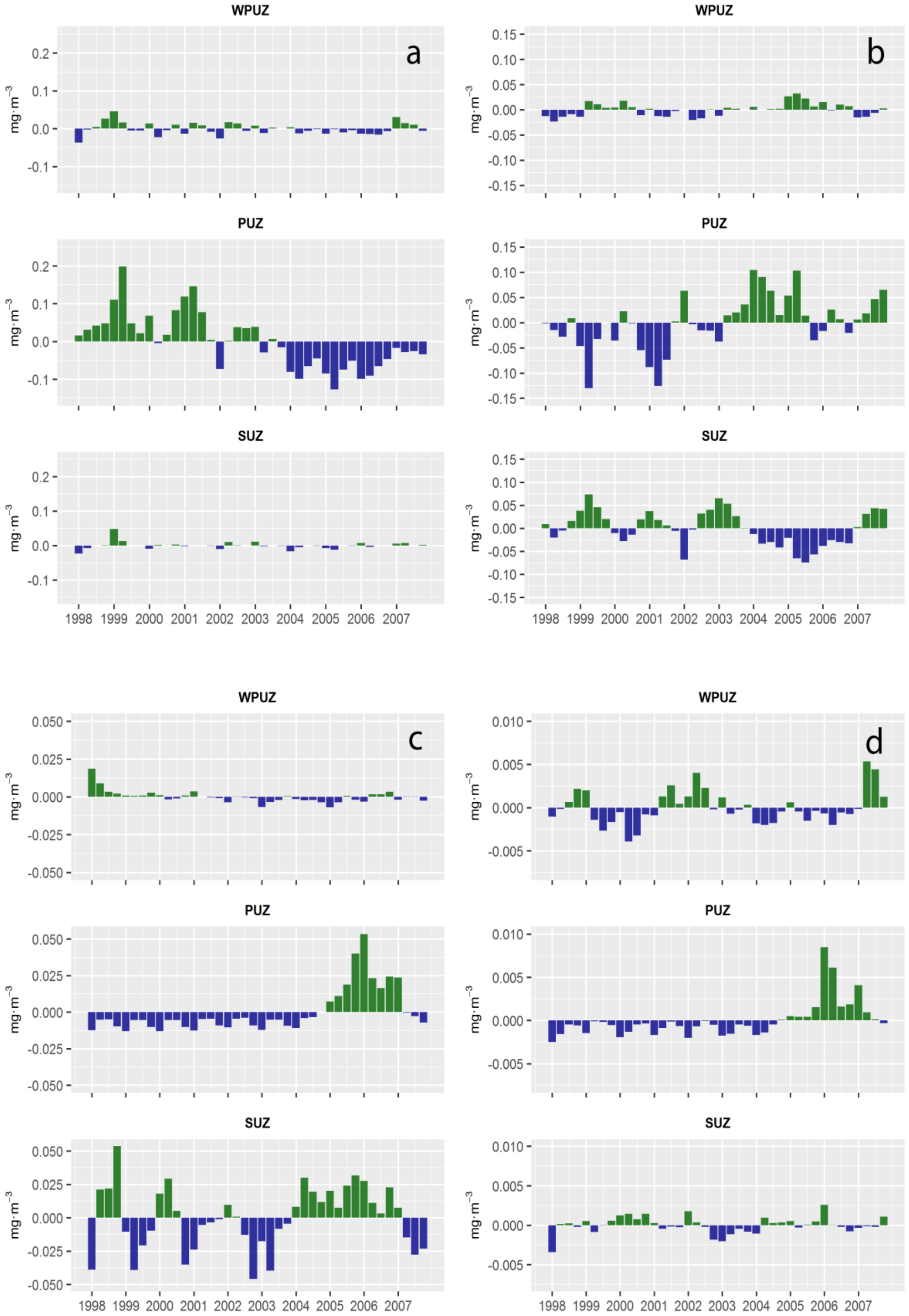

Fig. 9. Climatological anomalies of diatom (a), chlorophyte (b), cyanobacteria (c) and coccolithophore (d) concentrations (expressed in mgChl-a·m^{-3}) in each upwelling zone for the 1998-2007 period.

NPP (Fig. 10) and Chl-*a* (SF 5) also showed great spatial variability, with anomalies largely increasing southwards, from the WPUZ to the SUZ. The CbPM presented a singular anomaly pattern: inverse anomalies are registered in the SUZ relative to the PUZ and WPUZ. Moreover, the CbPM showed a very different pattern in their anomalies compared both to Chl-*a* and the Eppley-VGPM.

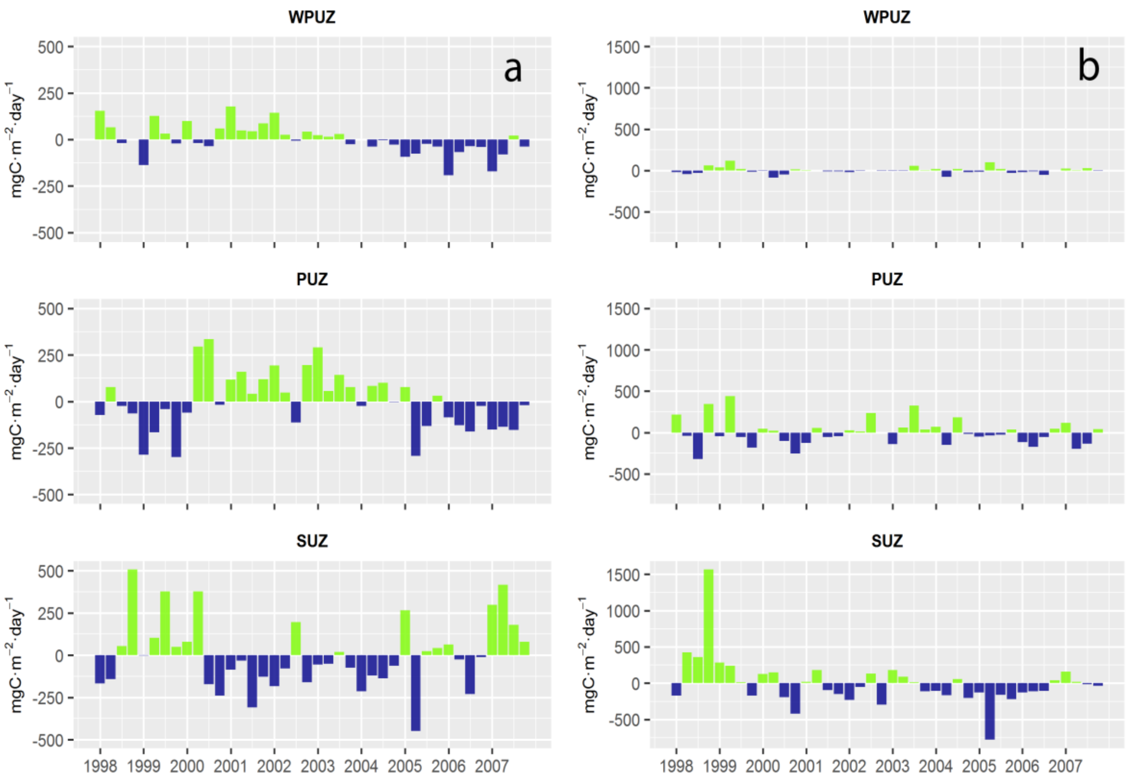

Fig. 10. Climatological anomalies of NPP, derived from the CbPM (a) and Eppley-VGPM (b) models in each upwelling zone for the 1998-2007 period.

Table 2 illustrates the correlations between NPP models and other variables at seasonal scales. Overall, the Eppley-VGPM was better correlated than the CbPM. Both models showed significant negative correlation with SST in the SUZ, where temporal variability is always stronger. The two models also correlated similarly with nutrients: they presented negative correlation with Fe and Si, and positive with nitrates and phosphates. The Eppley-VGPM showed a strong positive correlation (>0.8) with Chl-*a* (which was not unexpected, considering that the model is based on Chl-*a*), while the CbPM presented a weaker (although still significant) correlation in the SUZ. Regarding phytoplankton, the most remarkable positive correlations were between the two models and diatoms in the SUZ, which may suggest that increases of NPP in the highly-productive SUZ are driven by the growth of diatoms.

	Upwelling zone	NPP model	
		CbPM	Eppley-VGPM
SST	Weak permanent	0.16	-0.09
	Permanent	0.15	0.05
	Seasonal	*-0.32**	*-0.34**
Ekman pumping	Weak permanent	0.12	0.05
	Permanent	-0.12	0.13
	Seasonal	0.22	0.25
Fe	Weak permanent	0.11	**-0.54****
	Permanent	0.16	-0.12
	Seasonal	-0.14	-0.26
Si	Weak permanent	0.07	*-0.40**
	Permanent	-0.01	-0.03
	Seasonal	-0.04	-0.18
Nitrates	Weak permanent	*-0.34**	**0.48****
	Permanent	0.12	0.13
	Seasonal	0.13	0.26
Phosphates	Weak permanent	**0.59****	-0.18
	Permanent	*0.34**	0.07
	Seasonal	0.14	0.28
Chl	Weak permanent	0.17	**0.82****
	Permanent	0.10	**0.89****
	Seasonal	**0.43****	**0.93****
Diatoms	Weak permanent	0.03	**0.55****
	Permanent	0.09	0.06
	Seasonal	*0.39**	*0.36**
Coccolithophores	Weak permanent	0.01	0.17
	Permanent	**-0.46****	-0.15
	Seasonal	0.12	-0.22
Cyanobacteria	Weak permanent	0.29	0.08
	Permanent	-0.24	-0.06
	Seasonal	0.11	0.01
Chlorophytes	Weak permanent	-0.22	0.00
	Permanent	0.01	0.08
	Seasonal	0.28	**0.42****

Table 2. Correlations between seasonal climatological anomalies of the NPP models and the other variables for each of the upwelling zones. Significance of correlations is noted as follows: ($p<0.01$): **bold****; ($p<0.05$): *italics**.

3.3 Variability associated with climate modes

The degree of correlation between SST and various climate indices for the North Atlantic and Pacific Oceans, either considering or not a lag phase, are shown in Table 3. SST exhibited no significant correlation neither with the MEI nor with the SOI for any of the quarters of the year when a lag period was applied. However, when no lag was applied, significant negative (positive) correlations were present between SOI (MEI) and SST during winter and autumn for the WPUZ and PUZ (Table 3). On the other hand, neither NAO-SB, nor NAO-PC nor EA presented significant correlations for any of the analysed periods.

		Season			
	Upwelling zone	**Winter**	**Spring**	**Summer**	**Autumn**
NAO (SB)	**Weak permanent**	-0.0424	-0.3587	0.0729	*-0.6242**
	Permanent	-0.1515	-0.4559	0.2492	*-0.5758**
	Seasonal	-0.1030	*-0.6201**	0.2675	*-0.6364**
NAO (PC)	**Weak permanent**	0.2364	-0.3939	0.5030	-0.2364
	Permanent	-0.0061	-0.4182	0.6000*	-0.1394
	Seasonal	0.0788	-0.1152	0.4788	-0.2242
EA	**Weak permanent**	**0.7697****	0.2606	0.3818	0.0061
	Permanent	0.4909	0.1879	0.4424	-0.0788
	Seasonal	*0.5879**	0.1879	0.5152	-0.1636
SOI	**Weak permanent**	-0.5471	-0.0243	-0.3252	**-0.7697****
	Permanent	**-0.6565****	-0.2432	-0.4233	**-0.7576****
	Seasonal	-0.4985	0.2249	-0.5215	*-0.6000**
MEI	**Weak permanent**	0.5394	0.1879	0.2970	**0.6727****
	Permanent	**0.6970****	0.2606	0.4061	**0.6970****
	Seasonal	0.4061	-0.3818	0.4424	*0.5758**

Table 3. Correlations between seasonal SST anomalies and selected climate indices with no lag applied for the 1998-2007 period. Seasons correspond to the following months: JFM (winter), AMJ (spring), JAS (summer) and OND (autumn). Significance of correlations reads as follows: significant (p<0.05): **bold****; nearly significant (p<0.1): *italics**.

Nonetheless, when considering a longer data set (1993-2014), which is only available for SST, the result was completely different (Table 4). In this case there were significant negative correlations of SST with the Atlantic indices (NAO-SB and to a lesser extent NAO-PC), for winter, spring and autumn, especially at the PUZ and WPUZ. On the contrary, EA, SOI and MEI showed only sporadic significant or nearly significant correlations with SST.

		Season			
	Upwelling zone	**Winter**	**Spring**	**Summer**	**Autumn**
NAO (SB)	**Weak permanent**	**-0.5006****	**-0.4953****	0.0639	**-0.5919****
	Permanent	**-0.7034****	**-0.4360****	0.2368	**-0.7004****
	Seasonal	**-0.5785****	**-0.4298****	0.3396	**-0.4660****
NAO (PC)	**Weak permanent**	-0.1034	**-0.4558****	0.1768	**-0.5483****
	Permanent	*-0.3598**	**-0.4355****	0.1254	**-0.5968****
	Seasonal	-0.1875	-0.3440	0.0881	-0.3258
EA	**Weak permanent**	*0.4021**	-0.3587	0.1474	0.2524
	Permanent	0.2598	*-0.3824**	**0.4387****	0.1767
	Seasonal	0.3383	-0.1570	**0.5675****	0.0717
SOI	**Weak permanent**	-0.1322	0.1221	-0.1475	**-0.4997****
	Permanent	-0.1412	0.1210	0.2210	-0.2897
	Seasonal	-0.1553	*0.3817**	0.3149	0.0152
MEI	**Weak permanent**	0.2106	-0.0706	0.2185	*0.3676**
	Permanent	0.1903	-0.0186	-0.0864	0.1982
	Seasonal	0.1733	-0.3473	-0.2196	-0.0344

Table 4. Correlations between seasonal SST anomalies and selected climate indices with no lag applied for the 1993-2014 period. Seasons correspond to the following months: JFM (winter), AMJ (spring), JAS (summer) and OND (autumn). Significance of the correlations reads as follows: significant ($p<0.05$): **bold****; nearly significant ($p<0.1$): *italics**.

Regarding the other variables, Ekman pumping only exhibited few isolated significant correlations with these climate indices; nutrients displayed no clear patterns of correlation between them and the different climate indices; CbPM, Eppley-VGPM and SeaWiFS Chl-*a* showed only some occasional significant correlations; and phytoplankton groups, also exhibited only some sporadic significant correlations with the climate indices.

4. Discussion

Since Bakun (1990) proposed his upwelling intensification theory more than two decades ago it has become a matter of increasing interest especially in the last few years, as growing attention has been paid to global warming and more accurate satellite and model data have become available. Many studies have been published (see references in the following sections) addressing this subject, but it has not been possible to reach a consensus. Different results, both supporting and rejecting Bakun's hypothesis, suggest opposite trends even for the same EBUEs.

4.1 Linear trends

4.1.1 Trends in SST

Our computed SST trends reflect a non-surprising overall warming of the ocean, which has been extensively described in the bibliography over the last years (Levitus et al., 2000; Levitus et al., 2005; Hansen et al., 2006; Domingues et al., 2008; Hansen et al., 2010; Lyman et al., 2010; Gouretski et al., 2012). Nevertheless, warming trends calculated in the present work for this specific oceanic region are stronger than those found in the literature. Demarcq (2009) used AVHRR pathfinder v5 SST data to estimate trends for the same 1998-2007 period. Although the pattern is similar, his average trends were markedly smaller (up to half) than those obtained in the present work. This might be explained in part by the fact that he selected different areas to estimate the trends, but also because he used a different method for it (Least Absolute Deviations (LAD) instead of the Theil-Sen method employed here). Nevertheless, he obtained warmer trends when shelf waters were included in the estimates, a fact that qualitatively matches the findings presented here. This could mean that the open ocean waters are warming faster than those of the upwelling (especially in the SUZ, where large areas present non-significant changes) thus possibly suggesting an increase of upwelled, cool waters.

McGregor et al. (2007) examined two historical sediment cores (extending back 2500 years) from Cape Ghir, using the alkenone unsaturation index ($U_{37}^{K'}$) as a proxy for SST. For the most part of the 20th century the sediment cores showed a SST decrease of 1.2ºC. Narayan et al. (2010) also studied the Cape Ghir region within the CanC upwelling system as part of their analysis on SST and wind trends in the four major EBUEs. Comparing several wind datasets they obtained contradictory results on meridional wind trends, although the COADS (Comprehensive Ocean Atmosphere Dataset) data set, the most reliable to their view, exhibited an equatorward wind increase in the CanC. However, caution is required when extrapolating results from Narayan et al. (2010) to the whole CanC EBUE given that the SST upwelling index was estimated exclusively in the northern portion of the WPUZ and meridional wind stress time series correspond to a small region of 3ºx5º of a non-specified location within the upwelling system.

Barton et al. (2013) criticized the results of the abovementioned works. They argued that the use of $U_{37}^{K'}$ as a proxy of SST could lead to results biased towards lower SST because of coccolithophores (from which $U_{37}^{K'}$ signal is derived) living in deeper layers; i.e. as the ocean warms and stratifies, phytoplankton will tend to occupy deeper parts of the water column and in consequence have less contact with the mixed layer temperatures. Thus, estimating SST from $U_{37}^{K'}$ as McGregor et al. (2007) did would bias measures towards lower SSTs than the real ones, as results would truly correspond to cooler subsurface waters. As for Narayan et al. (2010), Barton et al. (2013) suggested that the evidence for increased upwelling (a greater SST difference between the coast and the open ocean) is not based on a cooling of the coastal waters but on a greater warming of the open ocean waters, as observed in the present work. Furthermore, Barton et al. (2013) analysed several wind and SST datasets and found that there were not significant changes in meridional wind intensity off NW Africa but a significant SST increase. Consequently, they did not find any strong evidence supporting Bakun's hypothesis.

Cropper et al. (2014) estimated SST trends from HadISST (Hadley Centre Sea Ice and Sea Surface Temperature) and OISST (Optimum Interpolation Sea Surface Temperature) datasets for the summer months (June to August), i.e., when the trade winds are strongest. Their findings showed a small negative SST trend for the PUZ, although the trend was not significant even at the 0.1 level. They also found a significant increase in the equatorward meridional wind in several datasets but, once again, the significance limit is set at the 0.1 level, challenging the interpretation of the results.

4.1.2 Trends in NPP and Chl-a

NPP and Chl-*a* can be used as a proxy for upwelling intensity because, although they depend on several factors, upwelling of deep waters is the primary driver of the amount of available nutrients for phytoplankton, which in turn control NPP and Chl-*a* amount (Ohde and Siegel, 2010; Messié and Chavez, 2015).

Trends for the times series of the two NPP models present quite different results. Seasonal to decadal changes in the Eppley-VGPM are nearly exclusively located around and south of Cape Blanc, and with the exception of some isolated patches they are not statistically significant. Furthermore, the PUZ and WPUZ exhibited no significant trends at all. This seems to indicate that no variation in upwelling intensity was experienced for the 1998-2007 period. On the contrary, the CbPM showed large areas with significant opposite trends. The sharp negative trends observed in the PUZ and WPUZ suggest an important decadal decrease in upwelling activity. Although assessing which of the two models behaves better in the CanC region is beyond the scope of the present work, there are some characteristics of the models' performance that are worth discussing.

The disagreement between the model outputs might arise from dissimilarities in the way the two models estimate NPP, as well as in errors from the input data. As mentioned by Kahru et al. (2009), the VGPM requires three input fields while the CbPM needs five, thus increasing uncertainties in derived NPP. Kahru et al. (2009) showed that in the California Current region the VGPM adjusted to in situ NPP measurements (obtained from the large CALCOFI data base) 27% better than the CbPM. However, in an ecosystem like the NW African coastal upwelling, where mixotrophy is a major feature of the planktonic community (Anabalón et al., 2014), Chl-*a* might not be the most adequate proxy to infer NPP: mixotrophic phytoplankton groups would contribute to increase C:Chl-*a* ratios, thus possibly biasing the output from NPP models based on Chl-*a*. On the other hand, it is worthwhile noting the qualitative differences between the Eppley-VGPM and Chl-*a* trends (Table 1 and Fig. 6), as concomitant variations would be expected considering that the former is derived from the latter. Remarkably, trend disparities only occur in the shelf portion of upwelling zones, where small positive Eppley-VGPM trends contrast with negative ones for Chl-*a*, especially in the SUZ. Conversely, slope and open ocean portions present similar trends for the two models. The exact reasons of these discrepancies are unknown but they might arise from biases in the models' input field data because a) discrepancies occur in coastal regions where satellite measures are most vulnerable and b) differences produced by the model structure itself would be expected to manifest everywhere.

The marked seasonality exhibited by NPP in WPUZ and PUZ initially might not seem to fit with the upwelling patterns described in classical and recent literature. Wooster et al. (1976) and Van Camp et al. (1991) mentioned three similar zones regarding trade wind seasonality: 1) strong, year-round trade winds between 20-25ºN, where permanent upwelling is present; 2) persistent trade winds during winter south of 20ºN, which fade during summer; and 3) persistent trade winds during summer north of 25ºN, which fade during winter. Cropper et al. (2014) followed a similar description except for the northernmost section of the upwelling system. North of 26ºN they describe the aforementioned weak permanent annual upwelling zone where, despite the fact that a maximum in upwelling intensity is registered during summer months, its occurrence is year-round. Messié and Chavez (2015) concluded that upwelled macronutrients (especially Si) for the most part of the year and light during winter control NPP in the CanC upwelling system. Hence, the clear seasonality of NPP in WPUZ and PUZ might be explained by the light cycle and the variation of the trade wind intensity between seasons. Thus, NPP changes could be attributable to the amount of light and strength of trade winds, whose intensity peaks during summer in the PUZ and WPUZ, when higher NPP are registered (in contrast to the SUZ, where NPP peaks during late winter and spring when upwelling intensity is maximum and fades in summer, following the wind patterns).

Demarcq (2009) estimated SeaWiFS Chl-*a* trends for the same period as in our study. They obtained similar trends, with small differences due to the different areas selected for trend averaging and the distinct methods used to calculate the trends (Theil-Sen method against LAD method). In the two cases the overall decreasing trend in Chl-*a* (and also in NPP derived from the Eppley-VGPM in our study) is less pronounced (or even positive) over the shelf. Demarcq (2009) suggested that this might be due to an increase in upwelling intensity or its intrinsic efficiency. However, he did not estimate the significance of the trend, which probably is not significant, as in our study (see SF 1c).

In summary, NPP and Chl-*a* trends exhibit heterogeneous patterns depending on the upwelling portion and/or production model analysed, but without any significant increasing trend, challenging Bakun's hypothesis. Our results support the studies of Gómez-Gesteira et al. (2008) and Barton et al. (2013), but disagree with those of McGregor et al. (2007), Narayan et al. (2010) and Cropper et al. (2014).

4.1.3 Trends in phytoplankton groups

Phytoplankton concentrations derived from the NOBM showed a marked change in group distributions, with some groups substituting others. Although this is in part due to the nature of the model itself (it represents phytoplankton groups as fractions of a total), the fact that the presence of some groups is diminishing in some areas and flourishing in others might indicate a change in environmental conditions. The decrease of diatoms in the PUZ may be produced by a weakening of upwelling intensity, as diatoms tend to dominate in more turbulent, nutrient-rich waters but struggle in more stable conditions, giving way to groups like dinoflagellates or haptophytes (represented here by chlorophytes), as is the case.

However, caution is required with these results. In addition to its limited spatial resolution, the fact that the NOBM is a global model could make results from regional areas not to entirely adjust to real conditions, even more considering the complexity of coastal areas.

4.2 Seasonal climatological anomalies

The spatial variability of the anomalies between the three upwelling areas gives a good insight into the different behaviours of the zones of the system. In general, WPUZ and PUZ exhibit similar patterns whereas SUZ usually differs from the formers. CbPM is a clear example: anomalies in the SUZ are opposing to those in the WPUZ and PUZ. Indeed, the upwelling regime of the two northern sections of the system is relatively similar and stable throughout the year, in contrast to the highly variable SUZ. These latitudinal differences suggest that the CanC upwelling system might not respond homogeneously to environmental changes, implying that differences in the evolution of the upwelling zones could be expected in the future.

There is great heterogeneity between the different subregions regarding the extent of the anomalies of each group, which is in part explained by the distinct characteristics of the groups and of the selected areas themselves (Fig. 2).

SST is expected to negatively correlate to NPP, as the former is inversely related to upwelling intensity, which is the main driver of NPP upwelling system by injecting cold, nutrient-rich deep waters into the surface (Messié and Chavez, 2015). However, significant correlations between SST and NPP were only found in the SUZ, where changes in upwelling intensity are stronger. Moreover, correlations between NPP models and nutrients showed ambiguous results. The fact that NPP is negatively related to Si and Fe in a significant way is clearly counterintuitive. A positive relation could be expected between NPP and a nutrient or, at worst, an absence of correlation if the nutrient does not limit NPP. This apparent lack of coherence in the relation could possibly arise from the nutrient model which would not correctly reproduce real distribution and abundance of those nutrients. Regarding phytoplankton groups, the positive (negative) correlation between NPP and diatoms (coccolithophores) could be explained by the preferred conditions of each group, as diatoms (coccolithophores) tend to inhabit upwelled (open-ocean) waters, where NPP is higher (lower).

4.3 Variability associated with climate modes

The correlation between the different indices and SST is linked by the intensity of trade winds. Stronger trade winds yield greater upwelling intensity which in turn provokes lower SST. Thus, the observed negative (positive) correlation with SOI (MEI) would be explained by an atmospheric bridge between the Pacific and Atlantic oceans that regulated the upwelling favourable winds, as suggested by Arístegui et al. (2006) and Roy and Reason (2001). Nevertheless, while in these studies the correlation is observed applying a seasonal time-lag between the Pacific and Atlantic variability, in our study the stronger correlations are observed with no temporal delay. Likewise, the negative correlation between NAO and SST would work in a similar manner as positive (negative) values of NAO are associated with an intensification (reduction) of upwelling favourable winds and, consequently, with a decrease (increase) of SST in the upwelling area, as mentioned by Arístegui et al. (2006) and Cropper et al. (2014).

However, depending on the time-span selected for the analysis (1998-2007 or 1993-2014) stronger significant correlations are found either with the ENSO (1998-2007) or the NAO (1993-2014). This poses the question of whether correlations with the SOI/MEI indices are flawed by short-term changes. Results from the 1993-2014 period are preferably taken into account, which qualitatively agree with the evidence found by Cropper et al. (2014) that showed that significant correlation was present between upwelling intensity and NAO, but was not with ENSO. Cropper et al. (2014) defined the upwelling intensity using two upwelling indices: one derived from wind stress (UI^{W}) and the other inferred from the difference in SST between the coast and the open ocean (UI^{SST}). They only found a significant correlation between UI^{W} and NAO, but not with UI^{SST}. Similarly, Benazzouz et al. (2014) and Narayan et al. (2010) concluded that a significant correlation was absent between UI^{SST} and NAO. This could mean that, although UI^{SST} is a qualitatively acceptable index to characterise upwelling intensity (as suggested by Cropper et al., 2014), it lacks the ability to fully describe upwelling variability, perhaps due to its intrinsic simplicity and vulnerability to suffer variations caused by factors unrelated to upwelling, e.g., open ocean warming episodes.

The results from the correlations between NPP/Chl-*a* and the climate indices are unclear. As upwelling intensity is the main driver of Chl-*a* (Ohde and Siegel, 2010) and it is significantly correlated with climate modes, a similar coherent pattern would be expected with NPP/Chl-*a*. However, only a few isolated significant correlations were found and some of them are even counterintuitive (less NPP/Chl-*a* with increased upwelling intensity). This might be, once again, consequence of the short time period (1998-2007) for which data was analysed.

Regarding phytoplankton, the most remarkable results were the significant correlations observed between ENSO and diatoms/chlorophytes. Diatoms showed a positive (negative) correlation with SOI (MEI), which could be due to the effect of ENSO in the trade winds regime: an increase in alongshore wind speed would enhance upwelling intensity, providing the preferred conditions by diatoms (turbulent, nutrient-rich waters). On the contrary, chlorophytes, which are intended to represent small flagellates, exhibit an inverse relation with ENSO as they tend to be more abundant in stratified, nutrient-depleted waters.

5. Conclusions

The principal aim of the present work was to analyse the regional variability and interannual trends of NPP in the CanC upwelling region. Trends estimated for the 1998-2007 period showed differences between upwelling zones but in any case presented an increase over time, challenging the hypothesis formulated by Bakun (1990) of upwelling intensification under global warming. An unexpected result was that the two NPP models (CbPM and Eppley-VGPM) yielded qualitatively different average results for upwelling zones, as well as different interannual trends. While the CbPM exhibited marked, significant decreases in the shelf region of the WPUZ and PUZ, the Eppley-VGPM showed non-significant, subtle changes. Modelled NPP and *in situ* data comparisons carried out in the California Current have shown that the VGPM correlates better with *in situ* measurements than the CbPM. Although this could also be true for the CanC, it cannot be guaranteed due to differences in upwelling drivers and community structure between the two upwelling ecosystems (Messié and Chavez, 2015). Consequently, a similar comparative analysis would be needed for the CanC upwelling region to elucidate which model reproduces better the actual variability in NPP.

Like with interannual trends, seasonal anomalies exhibited sub-regional variability, emphasising the importance of analysing local factors at each subregion. The correlation between NPP anomalies and other variables (e.g. with nutrients) produced some unexpected and ambiguous results, which could be attributed, at least in part, to the accuracy and resolution of the models.

The variability associated with climate modes could be of importance to predict future perturbations in the CanC EBUE, as changes in wind patterns related to variations of climate indices seem to regulate upwelling intensity. An individualized study for each season has proved crucial in this aspect as distinct responses have been registered depending on the period of the year. The ambiguous results obtained in the present work, together with the absence of consensus in bibliography, do not allow to draw clear conclusions, probably due to the short period of time analysed.

Finally, the results from the present work need to be interpreted with caution, since extrapolating to longer periods can be misleading (as observed in the case of SST). Although long SST time series are relatively common, this is not the case for variables such as satellite-derived Chl-*a* or NPP. The only recent availability of satellite measurements combined with the use of different sensors, e.g., CZCS, SeaWiFS and MODIS, has limited the length of time series for variables such as Chl-*a* and NPP to roughly a decade. Several approaches have been developed in order to merge some of these datasets (Antoine et al., 2005; Franz et al., 2005; Maritorena and Siegel, 2005; Gregg et al., 2010) with promising results, but not free of criticism (e.g. Chavez et al., 2011). Further improvements on NPP models and approaches to combine different Chl-*a*/NPP datasets, along with recent, more accurate data sets, will help to build climate data records of satellite-derived biological parameters, eventually allowing for a better comprehension of the evolution of upwelling ecosystems in a climate warming scenario.

Acknowledgements

The author of the present work would like to express his deepest gratitude to his tutors, Dr. J. Arístegui and Dr. A.J. González Ramos, for their continuous support and insightful advices during the realization of the work. Moreover, their thorough reviews of the manuscript profoundly improved it until reaching the final version. I would also like to praise Dr. J. Coca for selflessly supplying Ekman pumping data and helping me with part of the data analysis. Finally, I would like to thank the other data providers mentioned in the *Methods* section for freely providing the datasets employed here.

References

Anabalón, V., Arístegui, J., Morales, C.E., Andrade, I., Benavides, M., Correa-Ramírez, M.A., Espino, M., Ettahiri, O., Hormazabal, S., Makaoui, A., Montero, M.F., Orbi, A., 2014. The structure of planktonic communities under variable coastal upwelling conditions off Cape Ghir (31ºN) in the Canary Current System (NW Africa). Progress in Oceanography 120, 320–339.

Antoine, D., Morel, A., Gordon, H.R., Banzon, V.F., Evans, R.H., 2005. Bridging ocean color observations of the 1980s and 2000s in search of long-term trends. Journal of Geophysical Research 110, C06009.

Arístegui, J., Álvarez-Salgado, X.A., Barton, E.D., Figueiras, F.G., Hernández-León, S., Roy, C., Santos, A.M.P., 2006. Chapter 23: oceanography and fisheries of the Canary current/Iberian region of the eastern North Atlantic (18a,E). In A.R. Robinson and K.H. Brink (Eds.), *The Sea* 14, 877–931. Harvard, MA: Harvard University Press.

Arístegui, J., Barton, E.D., Álvarez-Salgado, X.A., Santos, A.M.P., Figueiras, F.G., Kifani, S., Hernández-León, S., Mason, E., Machú, E., Demarcq, H., 2009. Sub-regional ecosystem variability in the Canary Current upwelling. Progress in Oceanography 83, 33–48.

Aumont, O., Bopp, L., 2006. Globalizing results from ocean in situ iron fertilization studies. Global Biogeochemical Cycles 20, GB2017.

Aumont, O., Ethé, C., Tagliabue, A., Bopp, L., Gehlen, M., 2015. PISCES-v2: an ocean biogeochemical model for carbon and ecosystem studies. Geoscientific Model Development 8, 2465–2513.

Bakun, A., 1990. Global Climate Change and Intensification of Coastal Ocean Upwelling. Science 247, 198–201.

Barton, E.D., Field, D.B., Roy, C., 2013. Canary current upwelling: More or less? Progress in Oceanography 116, 167–178.

Behrenfeld, M.J., Falkowski, P.G., 1997a. Photosynthetic rates derived from satellite-based chlorophyll concentration. Limnology and Oceanography 42, 1–20.

Behrenfeld, M.J., Boss, E., Siegel, D.A., Shea, D.M., 2005. Carbon-based ocean productivity and phytoplankton physiology from space. Global Biogeochemical Cycles 19, GB1006.

Behrenfeld, M.J., O'Malley, R.T., Siegel, D.A., McClain, C.R., Sarmiento, J.L., Feldman, G.C., Milligan, A.J., Falkowski, P.J., Letelier, R.M., Boss, E.S., 2006. Climate-driven trends in contemporary ocean productivity. Nature 444, 752–755.

Belkin, I.M., 2009. Rapid warming of Large Marine Ecosystems. Progress in Oceanography 81, 207–213.

Benazzouz, A., Mordane, S., Orbi, A., Chagdali, M., Hilmi, K., Atillah, A., Pelegrí, J.L., Demarcq, H., 2014. An improved coastal upwelling index from sea surface temperature using satellite-based approach – The case of the Canary Current upwelling system. Continental Shelf Research 81, 38–54.

Boyce, D.G., Lewis, M.R., Worm, B., 2010. Global phytoplankton decline over the past century. Nature 466, 591–596.

Carr, M.E., Kearns, E.J., 2003. Production regimes in four Eastern Boundary Current systems. Deap-Sea Research II 50, 3199–3221.

Chavez, F.P., Messié, M., 2009. A comparison of Eastern Boundary Upwelling Ecosystems. Progress in Oceanography 83, 80–96.

Chavez, F.P., Messié, M., Pennington, J.T., 2011. Marine Primary Production in Relation to Climate Variability and Change. Annual Review of Marine Science 2011. 3, 227–260.

Coca, J., Ramos, A.G., Redondo, A, 2006. Cálculo del bombeo de Ekman a partir de datos del dispersómetro de viento SeaWindS abordo del satélite QuikSCAT. Revista de Teledetección, special number, 40–44.

Cropper, T.E., Hanna, E., Bigg, G.R., 2014. Spatial and temporal seasonal trends in coastal upwelling off Northwest Africa, 1981–2012. Deep-Sea Research I 86, 94–111.

Demarcq, H., 2009. Trends in primary production, sea surface temperature and wind in upwelling systems (1998–2007). Progress in Oceanography 83, 376–385.

Domingues, C.M., Church, J.A., White, N.J., Gleckler, P.J., Wijffels, S.E, Barker, P.M., Dunn, J.R., 2008. Improved estimates of upper-ocean warming and multi-decadal sea-level rise. Nature 453, 1090–1093.

Eppley, R.W., 1972. Temperature and phytoplankton growth in the sea. Fishery Bulletin 70, 1063–1085.

Franz, B.A., Bailey, S.W., Eplee Jr., R.E., Feldman, G.C., Kwiatkowska, E., McClain, C., Meister, G., Patt, F.S., Thomas, D., Werdell, P.J., 2005. The continuity of ocean color measurements from SeaWiFS to MODIS. Proceedings of SPIE - The International Society for Optical Engineering 5882, 304–316.

Gille, S.T., 2002. Warming of the Southern Ocean since the 1950s. Science 295, 1275–1277.

Gómez-Gesteira, M., de Castro, M., Álvarez, I., Lorenzo, M.N., Gesteira, J.L.G., Crespo, A.J.C, 2008. Spatio-temporal Upwelling Trends along the Canary Upwelling System (1967–2006). Annals of the New York Academy of Sciences 1146, 320–337.

Gouretski, V., Kennedy, J., Boyer, T., Köhl, A., 2012. Consistent near-surface ocean warming since 1900 in two largely independent observing networks. Geophysical Research Letters 39, L19606.

Gregg, W.W., 2008. Assimilation of SeaWiFS ocean chlorophyll data into a three-dimensional global ocean model. Journal of Marine Systems 69, 205–225.

Gregg, W.W., Casey, N.W., 2007. Sampling biases in MODIS and SeaWiFS ocean chlorophyll data. Remote Sensing of Environment 111, 25–35.

Gregg, W.W., Casey, N.W., 2010. Improving the consistency of ocean color data: A step toward climate data records. Geophysical Research Letters 37, L04605.

Gregg, W.W., Ginoux, P., Schopf, P.S., Casey, N.W., 2003. Phytoplankton and iron: validation of a global three-dimensional ocean biogeochemical model. Deep-Sea Research II 50, 3143–3169.

Hamed, K.H., Rao, A.R., 1998. A modified Mann Kendall trend test for autocorrelated data. Journal of Hydrology 204, 182–196.

Hansen, J., Sato, M., Ruedy, R., Lo, K., Lea, W., Medina-Elizade, M., 2006. Global Temperature Change. Proceedings of the National Academy of Sciences of the United States of America 103, 14288–14293.

Hansen, J., Ruedy, R., Sato, M., Lo, K., 2010. Global Surface Temperature Change. Reviews of Geophysics 48, RG4004.

Ihara, C., Kushnir, Y., Cane, M.A., 2008. Warming Trend of the Indian Ocean SST and Indian Ocean Dipole from 1880 to 2004. Journal of Climate 21, 2035–2046.

IPCC, 2014. Climate Change 2014: Impacts, Adaptation, and Vulnerability. Part A: Global and Sectoral Aspects. Contribution of Working Group II to the Fifth Assessment Report of the Intergovernmental Panel on Climate Change [Field, C.B., V.R. Barros, D.J. Dokken, K.J. Mach, M.D. Mastrandrea, T.E. Bilir, M. Chatterjee, K.L. Ebi, Y.O. Estrada, R.C. Genova, B. Girma, E.S. Kissel, A.N. Levy, S. MacCracken, P.R. Mastrandrea, and L.L. White (eds.)]. Cambridge University Press, Cambridge, United Kingdom and New York, NY, USA, 1132 pp.

Kahru, M., Kudela, R., Manzano-Sarabia, M., Mitchell, B.G., 2009. Trends in primary production in the California Current detected with satellite data. Journal of Geophysical Research 114, C02004.

Levitus, S., Antonov, J.I., Boyer, T.P., Stephens, C., 2000. Warming of the World Ocean. Science 287, 2225–2229.

Levitus, S., Antonov, J., Boyer, T., 2005. Warming of the world ocean, 1955–2003. Geophysical Research Letter 32, L02604.

Lyman, J.M., Good, S.A., Gouretski, V.V., Ishii, M., Johnson, G.C., Palmer, M.D., Smith, D.M., Willis, J.K., 2010. Robust warming of the global upper ocean. Nature 465, 334–337.

Maritorena, S., Siegel, D.A., 2005. Consistent merging of satellite ocean color data sets using a bio-optical model. Remote Sensing of Environment 94, 429–440.

Martinez, E., Antoine, D., D’Ortenzio, F., Gentili, B., 2009. Climate-Driven Basin-Scale Decadal Oscillations of Oceanic Phytoplankton. Science 326, 1253–1256.

McGregor, H.V., Dima, M., Fischer, H.W., Mulitza, S., 2007. Rapid 20th-Century Increase in Coastal Upwelling off Northwest Africa. Science 315, 637–639.

Messié, M., Chavez, F.P., 2015. Seasonal regulation of primary production in eastern boundary upwelling systems. Progress in Oceanography 134, 1–18.

Morel, A., 1991. Light and marine photosynthesis: a spectral model with geochemical and climatological implications. Progress in Oceanography 26, 263–306.

Narayan, N., Paul, A., Mulitza, S., Schulz, M., 2010. Trends in coastal upwelling intensity during the late 20th century. Ocean Science 6, 815–823.

Nieves, V., Willis, J.K., Patzert, W.C., 2015. Recent hiatus caused by decadal shift in Indo-Pacific heating. Nature 349, 532–535.

Oerder, V., Colas, F., Echevin, V., Codron, F., Tam, J., Belmadani, A., 2015. Peru-Chile upwelling dynamics under climate change. Journal of Geophysical Research: Oceans 120, 1152–1172.

Ohde, T., Siegel, H., 2010. Biological response to coastal upwelling and dust deposition in the area off Northwest Africa. Continental Shelf Research 30, 1108–1119.

Roy, C., Reason, C., 2001. ENSO related modulation of coastal upwelling in the eastern Atlantic. Progress in Oceanography 49, 245–255.

Sen, P.K., 1968. Estimates of the Regression Coefficient Based on Kendall's Tau. Journal of the American Statistical Association 63, 1379–1389.

Smith, W.H.F., Sandwell, D.T., 1997. Global sea floor topography from satellite altimetry and ship depth soundings. Science 277, 1956–1962.

Snyder, M.A., Sloan, L.C., Diffenbaugh, N.S., Bell, J.L., 2003. Future climate change and upwelling in the California Current. Geophysical Research Letters 30, 1823.

Sydeman, W.J., García-Reyes, M., Schoeman, D.S., Rykaczewski, R.R., Thompson, S.A., Black, B.A., Bograd, S.J., 2014. Climate change and wind intensification in coastal upwelling ecosystems. Science 345, 77–80.

Theil, H., 1950. A rank-invariant method of linear and polynomial regression analysis (I, II & III). Koninklijke Nederlandse Akademie Van Wetenschappen 53, 386–392, 521–525, 1397–1412.

Van Camp, L., Nykjae, L., Mittelstaedt, E., Schlittenhardt, P., 1991. Upwelling and boundary circulation off Northwest Africa as depicted by infrared and visible satellite observations. Progress in Oceanography 26, 357–402.

Varela, R., Álvarez, I, Santos, F., deCastro, M., Gómez-Gesteira, M., 2015. Has upwelling strengthened along worldwide coasts over 1982-2010? Scientific Reports 5, 10016.

Wang, D., Gouhier, T.C., Menge, B.A., Ganguly, A.R., 2015. Intensification and spatial homogenization of coastal upwelling under climate change. Nature 518, 390–394.

Westberry, T., Behrenfeld, M.J., Siegel, D.A., Boss, E., 2008. Carbon-based primary productivity modeling with vertically resolved photoacclimation. Global Biogeochemical Cycles 22, GB2024.

Wooster, W.S., Bakun, A., McLain, D.R., 1976. The seasonal upwelling cycle along the eastern boundary of the North Atlantic. Journal of Marine Research 34, 131–141.

Supplementary material

Acronyms and abbreviations

AMJ	April, May, June
AVHRR	Advanced Very High Resolution Radiometer
CanC	Canary Current
CbPM	Carbon-based Production Model
Chl-*a*	Chlorophyll-*a*
COADS	Comprehensive Ocean Atmosphere Dataset
CZCS	Coastal Zone Color Scanner
EA	Eastern Atlantic pattern
EBUE	Eastern Boundary Upwelling Ecosystem
ENSO	El Niño – Southern Oscillation
EOF	Empirical Orthogonal Function
Fe	Iron
HadISST	Hadley Centre Sea Ice and Sea Surface Temperature
JAS	July, August, September
JFM	January, February, March
LS	Least Squares
LAD	Least Absolute Deviation
MEI	Multivariate ENSO Index
MODIS	Moderate Resolution Imaging Spectroradiometer
NAO	North Atlantic Oscillation
NAO-PC	Principal Component-based North Atlantic Oscillation
NAO-SB	Station-based North Atlantic Oscillation
NCAR	National Center for Atmospheric Research
NOAA	National Oceanic and Atmospheric Administration
NOBM	NASA Ocean Biogeochemical Model
NPP	Net Primary Production
OISST	Optimum Interpolation Sea Surface Temperature
OND	October, November, December
OSU	Oregon State University
PAR	Photosynthetically Active Radiation
PISCES	Pelagic Interactions Scheme for Carbon and Ecosystem Studies
PUZ	Permanent Upwelling Zone
SeaWiFS	Sea-Viewing Wide Field-of-View Sensor
Si	Silica
SLP	Sea-level Pressure

SOI	Southern Oscillation Index
SST	Sea-surface Temperature
SUZ	Seasonal Upwelling Zone
UI^{SST}	SST-based Upwelling Index
UI^{W}	Wind-based Upwelling Index
VGPM	Vertically Generalized Production Model
WPUZ	Weak Permanent Upwelling Zone

Procedure to estimate Ekman pumping:

Ekman pumping was derived from wind speeds as follows: firstly, zonal (τ_x) and meridional (τ_y) wind stress components were calculated empirically:

$$\tau_x = \rho_a C_d \left(U_x^2 + U_y^2\right)^{1/2} U_x \ ; \ \tau_y = \rho_a C_d \left(U_x^2 + U_y^2\right)^{1/2} U_y \qquad (1)$$

where ρ_a is the air density (1.3 kg·m^{-3}), U_x and U_y the zonal and meridional wind speeds at 10 metres above sea level, respectively, and C_d the dimensionless drag coefficient, which can be related linearly to wind speed as follows: $C_d = a + bU$. a (0.0006) and b (0.00006 m^{-1}·s) are estimated empirically.

Balance between the Coriolis force and the vertical friction mixing of momentum is governed by the following expressions:

$$-fv = \frac{1}{\rho_w}\frac{\partial \tau_x}{\partial z} \ ; \ fu = \frac{1}{\rho_w}\frac{\partial \tau_y}{\partial z} \qquad (2)$$

where u and v are the zonal and meridional components of the water velocity, respectively, f is the Coriolis parameter (7.3 ·10^{-5} rad·s^{-1}) and ρ_w is the water density (1024.8 kg ·m^{-3}).

If the above equations are vertically integrated over the water column $\left(\int_{-\infty}^{0} dz\right)$ the result is the Ekman transport:

$$U_E = \frac{1}{\rho_w f}\tau_y \ ; \ V_E = -\frac{1}{\rho_w f}\tau_x \qquad (3)$$

where U_E and V_E are the zonal and meridional components of the Ekman transport, respectively. This implies that the depth integrated flow will be 90º to the right (left) of the wind stress in the NH (SH).

Depending on the wind patterns, convergence or divergence of Ekman transport may occur. Following the definition of divergence:

$$\frac{\partial U_E}{\partial x} + \frac{\partial V_E}{\partial y} = \frac{1}{\rho_w f}\frac{\partial \tau_y}{\partial x} - \frac{1}{\rho_w f}\frac{\partial \tau_x}{\partial y} = \frac{1}{\rho_w f}\left(\frac{\partial \tau_y}{\partial x} - \frac{\partial \tau_x}{\partial y}\right) \quad (4)$$

As $\frac{\partial \tau_y}{\partial x} - \frac{\partial \tau_x}{\partial y}$ is the z component of the wind rotational (wind curl), divergence/convergence will exist when wind curl is not equal to zero. This divergence/convergence of Ekman transport can be quantified by considering the equation of mass conservation:

$$\frac{\partial u}{\partial x} + \frac{\partial v}{\partial y} + \frac{\partial w}{\partial z} = 0 \;\rightarrow\; \int_{W_E}^{0} dw = -\int_{-\infty}^{0}\left(\frac{\partial u}{\partial x} + \frac{\partial v}{\partial y}\right) dz \quad (5)$$

where u, v and w are the three components of the water velocity and W_E is the vertical component of the Ekman transport due to divergence/convergence. Thus, integrating the above expression gives:

$$W_E = \frac{1}{\rho_w f}\left(\frac{\partial \tau_y}{\partial x} - \frac{\partial \tau_x}{\partial y}\right) \quad (6)$$

This implies that when wind curl is positive (negative) Ekman pumping (W_E) is consequently positive (negative), i.e., there is an upward (downward) transport of water.

Supplementary figures and tables

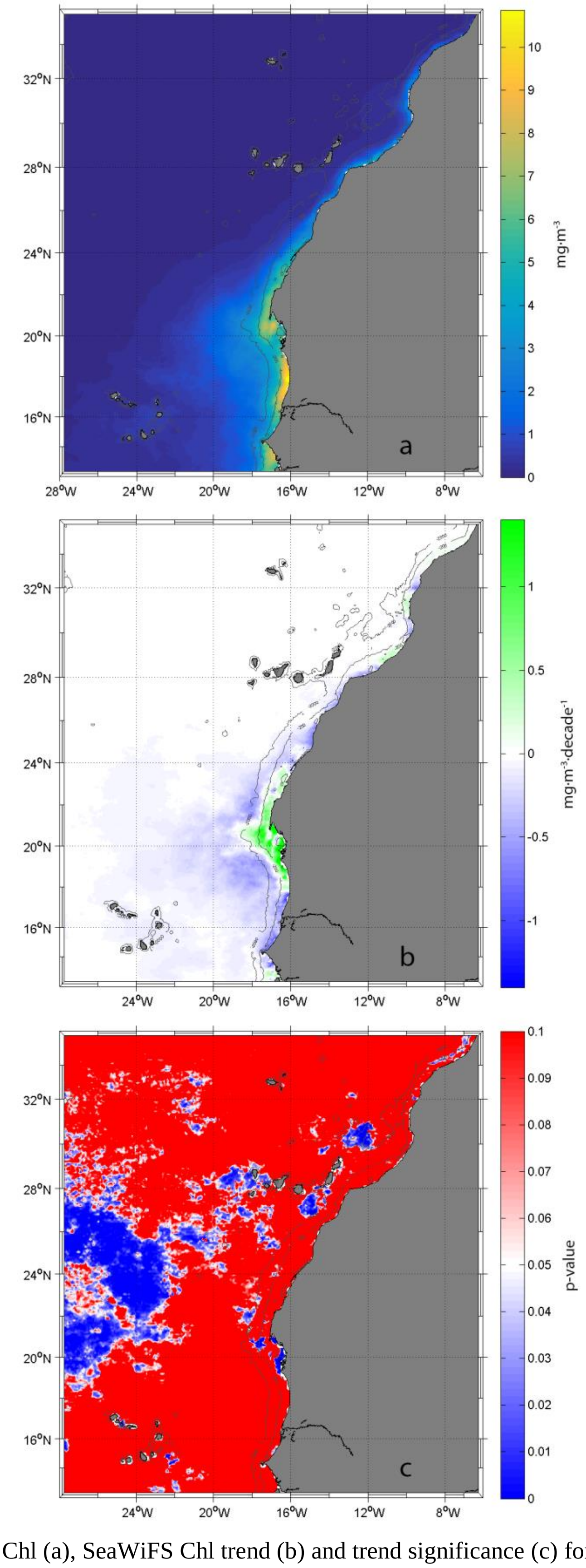

SF 1. Mean SeaWiFS Chl (a), SeaWiFS Chl trend (b) and trend significance (c) for the 1998-2007 period. In (c) blue corresponds to significant trend and red to non-significant trend. 200m and 2000m isobaths are represented by grey contour lines.

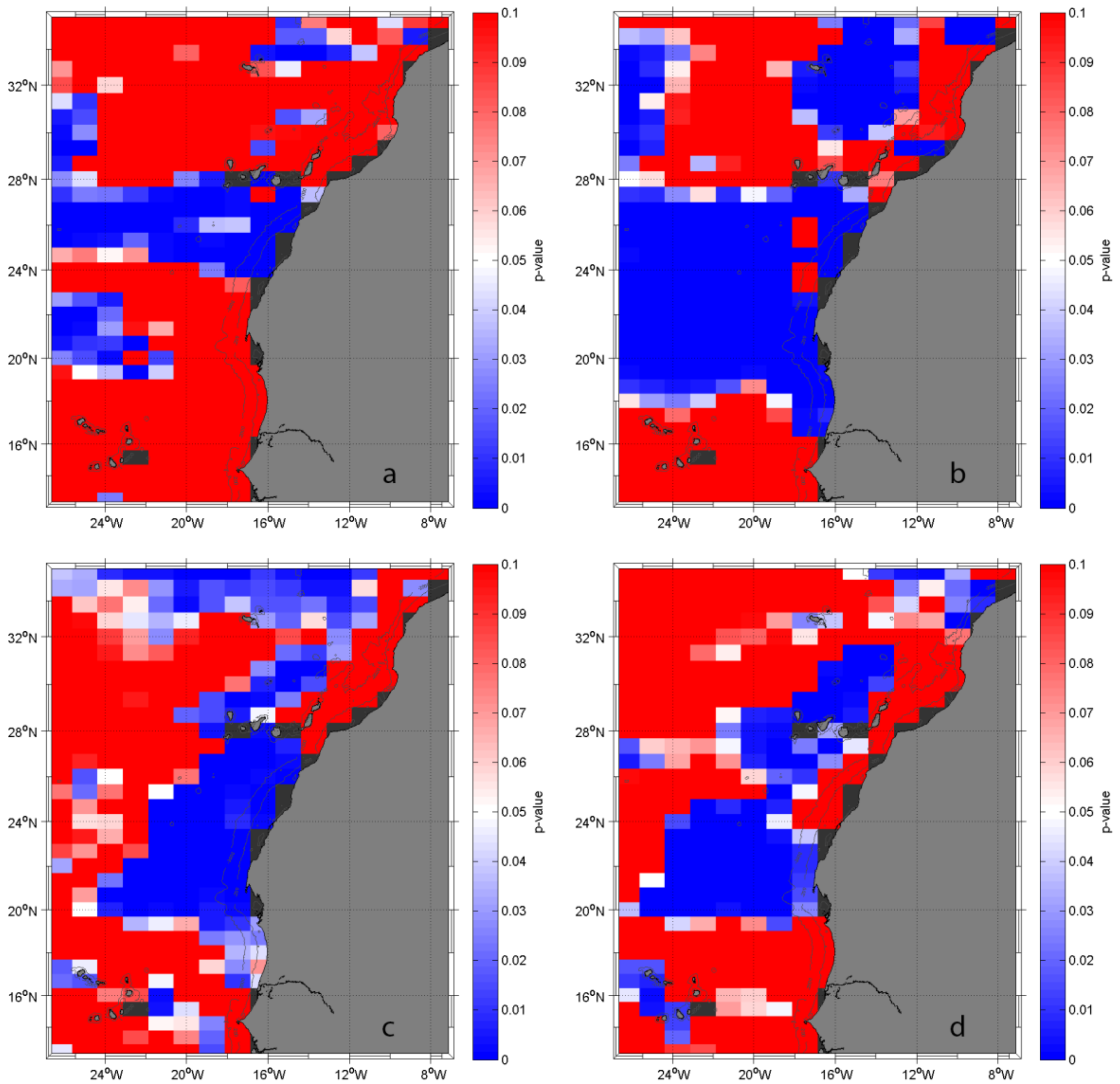

SF 2. Significance of trends in phytoplankton groups: diatoms (a), chlorophytes (b), cyanobacteria (c) and coccolithophores (d). Blue corresponds to significant trend and red to non-significant trend. 200m and 2000m isobaths are represented by grey contour lines.

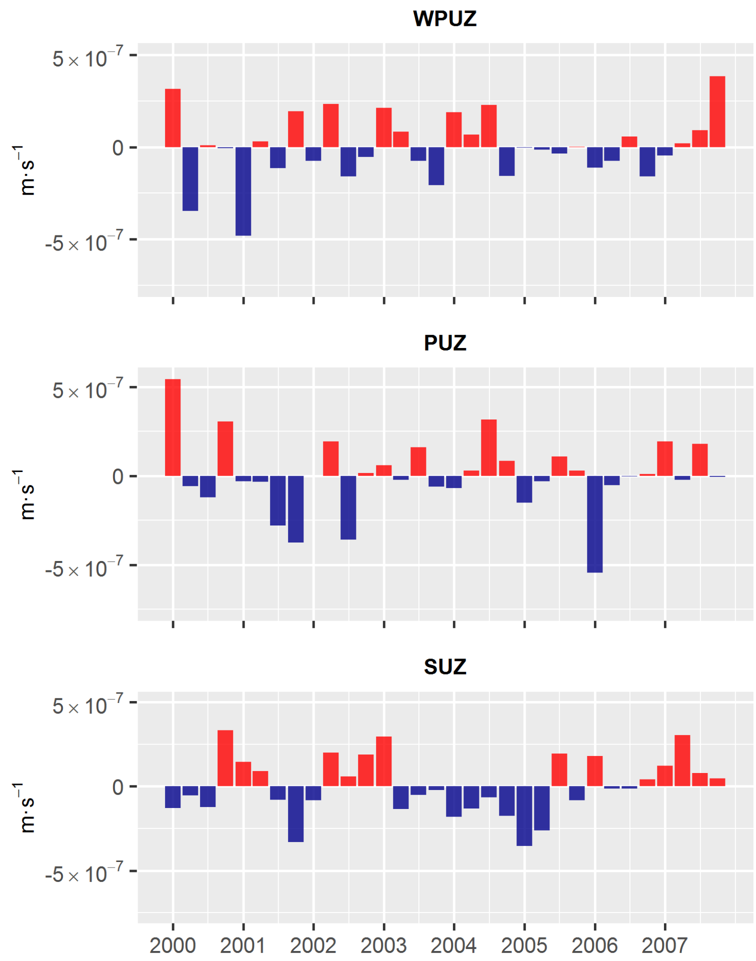

SF 3. Climatological anomalies of Ekman pumping in each upwelling zone for the 1998-2007 period.

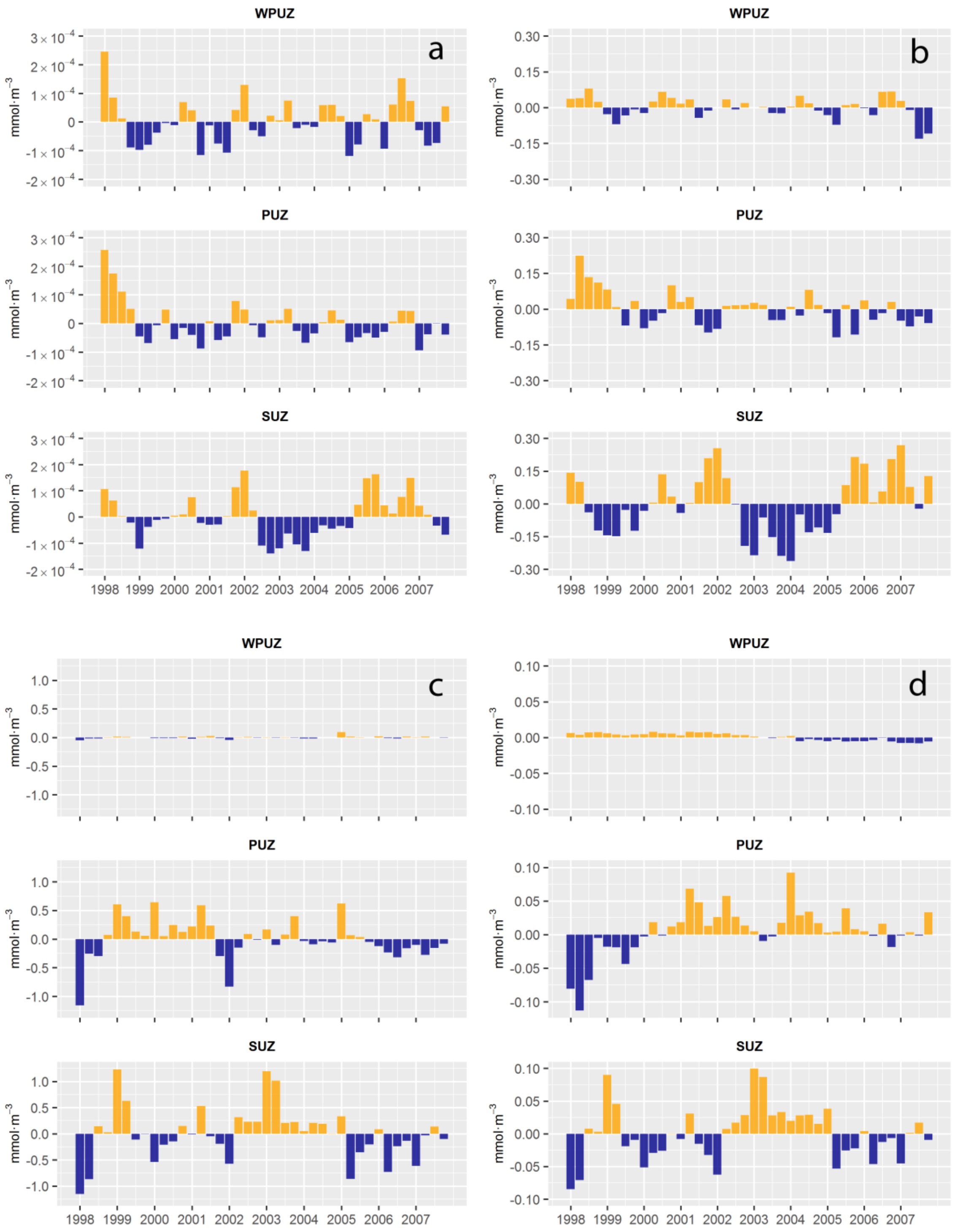

SF 4. Climatological anomalies of nutrient concentrations derived from the PISCES model in each upwelling zone for the 1998-2007 period. Iron (a), silicates (b), nitrates (c) and phosphates (d).

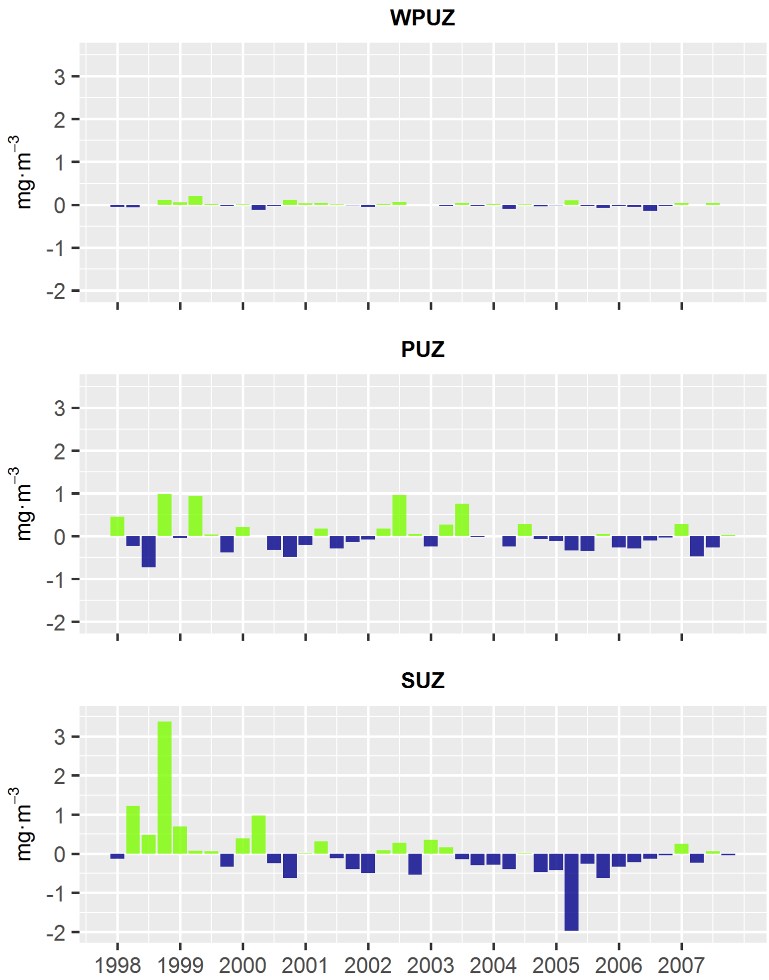

SF 5. Climatological anomalies of SeaWiFS Chl-*a* in each upwelling zone for the 1998-2007 period.

Descripción detallada de las actividades desarrolladas durante la realización del TFT

Las actividades realizadas durante el TFT se han centrado en la continuación de las tareas desarrolladas durante las prácticas externas, es decir, en el procesamiento y análisis de diversos tipos de datos de variables oceanográficas obtenidas por teledetección.

Procesamiento de los datos

Los datos descargados se encontraban listos para ser empleados. Sin embargo, sí que se realizaron modificaciones de algunos de ellos. Por una parte, modificaciones consistieron en un promediado para convertir los diferentes tamaños de las celdas a una malla común mediante la cual se pudieran comparar entre sí. Por otra parte, y dado que los datos también tenían resoluciones temporales diferentes, se llevaron a cabo promedios para hacer coincidir los pasos temporales.

El promedio de los datos consistió en hacer coincidir varias celdas pequeñas de cierta variable con una grande de otra, promediando las primeras y creando así una nueva malla que coincida con aquella de la segunda variable. Dada la heterogeneidad de las mallas de las diferentes variables y que las coordenadas de los nodos no siempre coincidían, se optó por promediar las celdas que más se acercaran a ello. Por otro lado, teniendo en cuenta la posibilidad de comparar muchas variables diferentes en un modelo, se dio prioridad a realizar el promedio para crear mallas del tamaño de aquella con peor resolución y, por tanto, limitante: la del modelo NOBM. Así, los promedios realizados fueron:

En el caso del promedio temporal se pasaron todos los datos a medias mensuales.

Análisis de datos

Para conocer con mayor detalle la forma en que las variables evolucionaban tanto espacial como temporalmente se calcularon las tendencias lineales de las variables mediante el método de Theil-Sen modificado para series con autocorrelación, haciendo uso de los datos de las series temporales completas de cada celda individual así como de promedios por zonas. Así fue posible crear mapas de tendencia que permitieron analizar la evolución de los valores que tomaban las variables en las diferentes subzonas de la región estudiada.

Los datos procesados tal y como se menciona en el apartado anterior se emplearon de varias formas. Por un lado, se compararon por pares para estudiar en qué grado estaban relacionadas entre sí. Para ello se realizó un ajuste lineal con cada pareja de variables y se calcularon el coeficiente de determinación del ajuste (R^2) y el coeficiente de correlación lineal de Pearson. En este último caso se conservaron tan solo los coeficientes estadísticamente significativos (esta estimación se realizó mediante el teste de la t de Student, estableciendo el límite de significancia en 0.05).

Se estimaron las anomalías climatológicas de las diferentes variables para cada estación del año. Con ellas se calcularon correlaciones mediante el método de la ρ de Spearman entre a) los datos de NPP y el resto; y b) índices climáticos y todas las variables.

Por otro lado, también se calculó un índice de afloramiento basado en la diferencia de temperatura entre la celda más cercana a costa y aquella 5º al oeste, en océano abierto, para cada latitud. Se empleó la climatología de la SST de cada semana, es decir, el promedio de SST de cada semana durante la serie temporal completa. Sin embargo, finalmente estos datos no fueron empleados en la versión final del TFT.

Finalmente, también se realizó un análisis wavelet (individual y cruzado) para analizar los periodos que dominan en cada variable, así como si estos periodos varían durante el tiempo o entre zonas. No obstante, al igual que en el caso anterior los resultados no se incluyeron en la versión final del TFT.

Lectura de bibliografía

A lo largo de la realización del TFT se llevó a cabo una extensa lectura de bibliografía relacionada con la materia de estudio.

Formación recibida

Durante la estancia en la institución se me proporcionó una breve formación en el empleo del software HDF View, el cual me fue de gran utilidad a la hora de trabajar con los datos, ya que permite la lectura y visualización de datos en formato HDF y NetCDF de forma rápida e intuitiva. De esta forma, me fue posible acelerar de forma sustancial los pasos de procesado y análisis de datos en Matlab, ya que previamente ya conocía la organización y estructura interna de los archivos.

Por otro lado, también tuve la oportunidad de adquirir conocimiento científico sobre diversos aspectos relacionados con el TFT.

Nivel de integración e implicación dentro del departamento y relaciones con el personal

Estimo que llegué a tener una alta integración e implicación dentro del departamento. Compartí despacho con dos miembros de la institución de forma que estos pudieron ayudarme en el transcurso del periodo de realización del TFT cuando necesitaba solventar dudas, siendo sus consejos de gran ayuda. Por si lo mencionado fuese poco, el hecho de proporcionarme los datos de bombeo de Ekman fue de inestimable ayuda.

Aspectos positivos y negativos más significativos relacionados con el desarrollo del TFT

Unos de los principales aspectos positivos significativos relacionados con el desarrollo del TFT fue la posibilidad de cumplir las expectativas que se tenía al comienzo. He adquirido nuevos e importantes conocimientos teóricos relacionados con el campo de la oceanografía basada en la teledetección, además de poder comprobar de primera mano cómo podría ser mi futuro si decidiera dedicarme a la investigación científica en este campo.

Otro aspecto positivo fue la integración con la parte del equipo del IOCAG y la división de robótica y oceanografía computacional del IUSIANI con la que tuve contacto. Desde el primer día estuvieron pendientes de mí y se mostraron dispuestos a ayudarme en todo lo que les era posible, tanto en lo referido a la realización del TFT en particular como la estancia misma en la institución. Gracias a ello el TFT pudo ser desarrolado de forma adecuada, cosa que hubiera sido imposible de otra forma.

Por otro lado, quisiera señalar que no he percibido ningún aspecto negativo significativo.

Valoración personal del aprendizaje conseguido a lo largo del TFT

Considero que, en general, el aprendizaje adquirido durante el desarrollo del TFT podría serme útil en un futuro, ya que he adquirido el conocimiento sobre cómo desarrollar un estudio científico. Por otro lado, y no menos importante, he podido aprender cómo plasmar en un artículo los resultados obtenidos en el estudio, al igual que discutirlos y resaltar las conclusiones más importantes que se derivan de ellos.

En particular, el conocimiento adquirido en datos de teledetección creo que es muy útil, ya que es un campo importante por el hecho de que proporciona una visión sinóptica del océano en el que se están dando notables avances.